

Sub-Ångström electrostriction in dielectric crystals

Citation for published version (APA):

Luymes, B. J. (1982). *Sub-Ångström electrostriction in dielectric crystals*. [Phd Thesis 1 (Research TU/e / Graduation TU/e), Electrical Engineering]. Technische Hogeschool Eindhoven. <https://doi.org/10.6100/IR147691>

DOI:

[10.6100/IR147691](https://doi.org/10.6100/IR147691)

Document status and date:

Published: 01/01/1982

Document Version:

Publisher's PDF, also known as Version of Record (includes final page, issue and volume numbers)

Please check the document version of this publication:

- A submitted manuscript is the version of the article upon submission and before peer-review. There can be important differences between the submitted version and the official published version of record. People interested in the research are advised to contact the author for the final version of the publication, or visit the DOI to the publisher's website.
- The final author version and the galley proof are versions of the publication after peer review.
- The final published version features the final layout of the paper including the volume, issue and page numbers.

[Link to publication](#)

General rights

Copyright and moral rights for the publications made accessible in the public portal are retained by the authors and/or other copyright owners and it is a condition of accessing publications that users recognise and abide by the legal requirements associated with these rights.

- Users may download and print one copy of any publication from the public portal for the purpose of private study or research.
- You may not further distribute the material or use it for any profit-making activity or commercial gain
- You may freely distribute the URL identifying the publication in the public portal.

If the publication is distributed under the terms of Article 25fa of the Dutch Copyright Act, indicated by the "Taverne" license above, please follow below link for the End User Agreement:

www.tue.nl/taverne

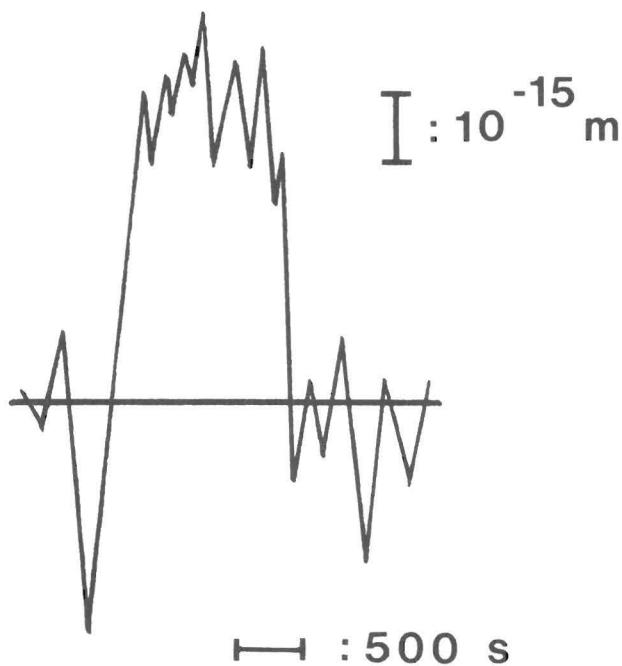
Take down policy

If you believe that this document breaches copyright please contact us at:

openaccess@tue.nl

providing details and we will investigate your claim.

SUB-ÅNGSTRÖM ELECTROSTRICTION IN DIELECTRIC CRYSTALS



B.J. LUYMES

DISSERTATIE DRUKKERIJ
wibro
HELMOND
TELEFOON 04920-23981

SUB-ÅNGSTRÖM ELECTROSTRICTION IN DIELECTRIC CRYSTALS

SUB-ÅNGSTRÖM ELECTROSTRICTION IN DIELECTRIC CRYSTALS

PROEFSCHRIFT

TER VERKRIJGING VAN DE GRAAD VAN DOCTOR IN DE
TECHNISCHE WETENSCHAPPEN AAN DE TECHNISCHE
HOGESCHOOL EINDHOVEN, OP GEZAG VAN DE RECTOR
MAGNIFICUS, PROF. DR. S. T. M. ACKERMANS, VOOR
EEN COMMISSIE AANGEWEEZEN DOOR HET COLLEGE
VAN DEKANEN IN HET OPENBAAR TE VERDEDIGEN OP
VRIJDAG 17 DECEMBER 1982 TE 16.00 UUR

DOOR

BERNEND JOHAN LUYMÉS

GEBOREN TE HUNTLY (NIEUW-ZEELAND)

Dit proefschrift is goedgekeurd
door de promotoren

Prof. Dr. F.N. Hooge

en

Prof. Dr. Th.G.M. Kleinpenning

CIP-gegevens

Luymes, Bernend Johan

Sub-Ångström electrostriction in dielectric crystals /

Bernend Johan Luymes. - [S.l. : s.n.]. Fig. -

Proefschrift Eindhoven. - Met lit. opg., reg.

ISBN 90-9000381-9

SISO 535 UDC 537.228 UGI 590

Trefw.: materiaalkunde.

CONTENTS

1	INTRODUCTION	
1.1	Small dilatations	1
1.2	Electrostriction	2
2	THE STABILIZED MICHELSON INTERFEROMETER	
2.1	Experimental set-up	5
2.2	Noise sources in the interferometer	14
2.3	Detection limit of the interferometer	27
2.4	Reference dilatation	29
2.5	Contracting or expanding sample	30
3	THEORY OF ELECTROSTRICTION	
3.1	An estimate of the electrostriction constant $ \gamma_{1111} $..	34
3.2	Relation between the dielectric constant and the electrostriction constant	41
4	ELECTROSTRICTION IN PRACTICE	
4.1	Sample requirements	45
4.2	Details on the preparation and mounting of the sample.	46
4.3	Experimental difficulties in measuring true electrostrictive dilatations	47
4.4	Non linearities introduced by the sinusoidal character of the interference relation	51
5	ELECTROSTRICTION IN LiF	54
6	ELECTROSTRICTION IN DIAMOND	
6.1	Information on the diamond samples	56
6.2	Estimate of γ_{1111} , using the crystal structure	58
6.3	Relation between γ_{1111} and the photo elastic constants	61
6.4	Measurement and conclusions	62

7	ELECTROSTRICTION IN QUARTZ	
7.1	Clamping of the sample by the support	66
7.2	Piezoelectric effect caused by second-harmonic distortion	75
7.3	Measurement of electrostriction in quartz	77
8	ELECTROSTRICTION IN TRIGLICINE SULPHATE (TGS)	
8.1	Information on TGS	80
8.2	Theory and measurements	82
8.3	Details on the adiabatic correction	88
9	SUMMARY AND CONCLUSIONS	90
	NOTATION INDEX	92
	REFERENCES	96
	TOELICHTING	100
	DANKWOORD	101
	CURRICULUM VITAE	102

1 Introduction

1:1 Small dilatations

Whether one considers a dilatation small depends largely on the subject one has in mind. This may vary from the dilatation of an expanding balloon to the dilatation of a pressed quartz crystal in a piezoelectric cigarette lighter. These dilatations are measured in m's and nm's, respectively. The scale of dilatations considered in this thesis is the atomic scale which is less than 1 nm.

An X-ray diffractometer¹ or a double-crystal neutron-diffractometer^{2,3} is able to detect steplike dilatations ΔL of 10 nm. For samples with a thickness L of about 1 cm this corresponds to a minimal detectable strain $\Delta L/L$ in the order of 10^{-6} . Dilatations of these order of magnitude occur in thermal expansion experiments.

Much smaller dilatations with an amplitude $\hat{\Delta L}$ of 1 pm can be detected by a capacitance dilatometer⁴ or an optical stabilized Michelson interferometer⁵. The corresponding detectable strains are of the order of 10^{-10} . Acoustic and thermal random dilatations, that occur in these instruments, can be compensated by an electronic servo loop^{6,7}. This enables precise measurements of $\hat{\Delta L}$ down to 0.1 pm and the detection of even smaller values of $\hat{\Delta L}$.

In this thesis we are concerned with measurements in the 0.1 pm (10^{-13} m) region. We used an interferometer capable of detecting dilatations in the order of 10^{-14} m or 10 fm.

1:2 Electrostriction

Small expansions in materials are expected in measurements of electrostriction. Electrostrictive strains $\Delta L_i/L_j$ ($i, j = 1, 2, 3$), which occur in every material when an electric field is applied, are proportional to products $P_k P_l$ ($k, l = 1, 2, 3$) of polarisation components P_i (C/m^2). The polarisation $\vec{P} = (P_1, P_2, P_3)$. The components P_1 , P_2 and P_3 lie along the x, y and z-axis, respectively. These axes form an orthogonal basis. This basis is shown in figure 1.1 together with the orientations and definitions of the dilatations ΔL_i and the lengths L_i .

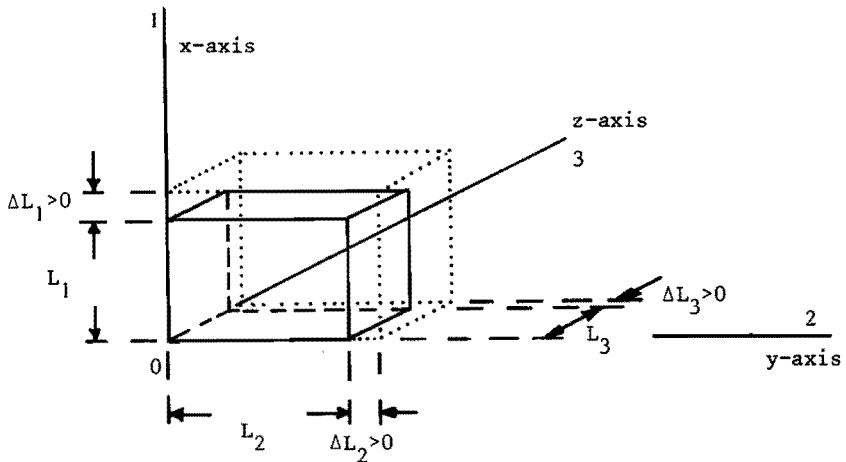


Figure 1.1 Definition of L_i and ΔL_i in relation with the orthogonal basis (x, y, z).

The constants relating $\Delta L_i/L_j$ to $P_k P_l$ form a fourth-rank tensor Q_{ijkl} (m^4/C^2). According to Devonshire⁸ electrostriction is described by

$$\Delta L_i/L_j = Q_{ijkl} P_k P_l \quad (1.1)$$

In the above equation the Einstein summation convention has been used.

Electrostrictive strains are generated by applying an electric field with components E_i (V/m) to a dielectric sample. So these strains may be described alternatively by⁹

$$\Delta L_i / L_j = \gamma_{klij} E_k E_l \quad (1.2)$$

where γ_{ijkl} (m^2/V^2) is a fourth-rank electrostriction tensor. This tensor is related to Q_{ijkl} by the dielectric tensor P'_{ij} (F/m) since $P_i = P'_{ij} E_j$. In this work γ_{ijkl} is measured according to (1.2). Equation (1.2) defines the electrostriction tensor γ_{ijkl} .

Relatively large values of P_i can be found in ferroelectric materials so these were the materials in which electrostriction was first investigated^{10,11}.

For instance, in triglycine sulphate (TGS) Q_{2222} was determined indirectly by measuring P_2 and g_{222} (m^2/C). The following equation defines g_{222}

$$g_{222} = \frac{\partial}{\partial P_2} (\Delta L_2 / L_2) \quad (1.3)$$

In general the piezoelectric tensor g_{ijk} is defined by the following relation⁸

$$g_{kij} = \frac{\partial}{\partial P_k} (\Delta L_i / L_j) \quad (1.4)$$

Since P_1 and P_3 may be assumed to be zero in TGS, it follows from (1.1) and (1.3) that $Q_{2222} = 4g_{222}/P_2$ in TGS.

Important relations leading⁹ to the value of γ_{ijkl} are:

$$\gamma_{ijkl} = \frac{\partial}{\partial E_j} (d_{ikl}), \text{ with } d_{ikl} = \frac{\partial}{\partial E_i} (\Delta L_k / L_l) \text{ and} \quad (1.5)$$

$$\gamma_{ijkl} = \frac{1}{2} \frac{\partial p'_{ij}}{\partial \sigma_{kl}} \quad (1.6)$$

d_{ijk} (m/V) is a piezoelectric tensor component and σ_{ij} (N/m²) a stress tensor component. Equations (1.4) and (1.5) are phenomenological relations. Equation (1.6) is a thermodynamic relation explained in section 3.2.

Pure electrostrictive strains were measured on NaCl, quartz¹² and TGS¹³ (about 1960). The sensitivity of the equipment used is 10-100 pm. Apparatuses with higher sensitivities as mentioned in section 1:1 allow electrostriction measurements in all dielectric materials.

Values of γ_{ijkl} can be predicted according to the phenomenological relation (1.5). Values of Q_{ijkl} are found by combining the phenomenological relations (1.1) and (1.4). Equation (1.6) leads to the exact value of γ_{ijkl} since it is a thermodynamical one.

In this thesis the direct measurements of γ_{iiii} with a stabilized Michelson interferometer are compared with the calculated results of (1.6).

Parameters related to electrostriction are the derivatives of both the dielectric constant¹⁴ and the refractive index¹⁵ with the respect to pressure. This is shown in principle by (1.6).

2 The stabilized Michelson interferometer

2:1 Experimental set-up

The experimental set-up is described in the following article which will be published in January 1983 by the journal "Review of Scientific Instruments".²⁹

Interferometric measurements of very small electrostrictive strains

B.J. Luymes

Eindhoven University of Technology, Department of Electrical Engineering,
5612 AZ Eindhoven. The Netherlands

Abstract

Electrostrictive dilatations in the order of 10^{-13} m are measured in dielectric crystals by an interferometric method based on the Michelson interferometer. The electrostriction constants γ_{1111} of quartz, diamond and of LiF are found to be (-0.6 ± 0.2) , $(+0.17 \pm 0.03)$ and $(-7.9 \pm 0.8) \cdot 10^{-21} \text{ m}^2/\text{V}^2$, respectively.

Introduction

An electronical-stabilized-Michelson interferometer has been built and adapted to measuring small electrostrictive AC dilatations ΔL_1 of a sample. ΔL_1 is in the order of 10^{-13} m. We use phase sensitive detection. The electronic stabilisation reduces the effects which mechanical-and accoustic-noise have on the sensitivity of the Michelson interferometer. This sensitivity is now 5×10^{-15} m. Small electrostriction constants γ_{1111} ($\approx 10^{-22} \text{ m}^2/\text{V}^2$) can now be measured on samples with a thickness L_1 ($\approx 10^{-3}$ m). There is no risk of electric breakdown through the air which could occur at electric fields E_1 greater than 1000V/mm. We started from the expression for the electrostrictive strain²

$$\Delta L_1/L_1 = \gamma_{1111} E_1^2 \quad (1)$$

where γ_{1111} is a component of the fourth-rank electrostriction tensor γ_{ijkl} . This expression defines γ_{1111} which is measured according to the method described below.

Experimental method

The measurements determining γ_{1111} will be described on the basis of the set-up given in Fig. 1. The interferometer shown in this figure is capable of measuring AC dilatations of a sample attached to mirror 1. These dilatations must be much smaller than 632.8 nm (the laserlight wavelength λ of the He-Ne laser). A zero-order interference spot is projected on the photodiode. The maximum

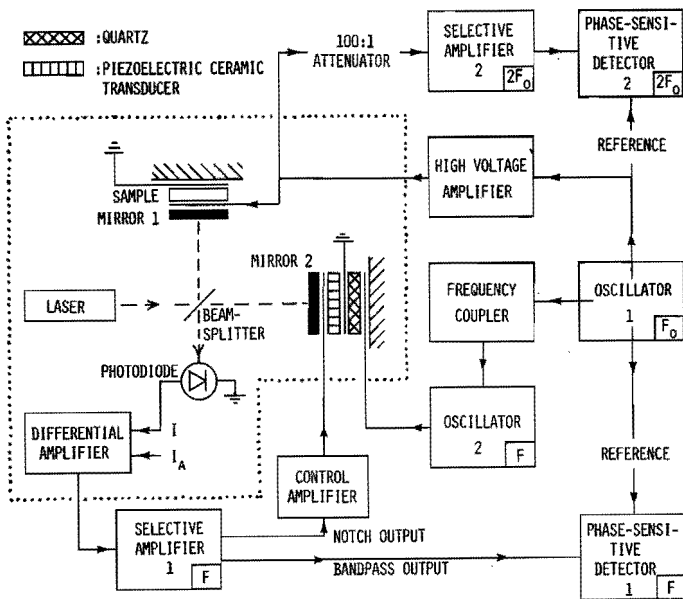


Figure 1 Schematic diagram of the stabilized Michelson interferometer adapted to measure electrostriction. The dotted area is the interferometer table. The frequency in the right hand corner of several blocks shows the tuning of these instruments. f can be either f_0 or $2f_0$.

sensitivity of this interferometer is obtained if the optical path-length difference (o.p.d.) between the two arms of the interferometer equals $\frac{1}{2}\lambda$ (disregarding $N\lambda$; $N = +1, +2, +3, \dots$). At this point the luminous intensity of the interference spot results in an electrical current $\frac{1}{2}(I_{\max} + I_{\min}) = I_a$ in the photodiode. The maximum (minimum) luminous intensity corresponds to the current I_{\max} (I_{\min}) and an o.p.d. of $\lambda(\frac{1}{2}\lambda)$.

From the measurements of I_{\max} and I_{\min} we determine I_a . The luminous intensity on the photodiode results in a current I proportional to the intensity. I consists of three parts: a DC current I_a , noise (which has a DC Component) and a signal current I_f with a frequency f . I_f contains the information about the dilatation of the sample. The differential amplifier determines the difference between I and a preset DC reference current I_a . Its output gives I_f superimposed on the noise component. The noise is given by the notch output of selective amplifier 1 which is tuned to f . This notch output is connected to the control amplifier which drives the piezoelectric ceramic transducer attached to mirror 2. The control amplifier is a proportional integrating lowpass amplifier. It has been designed to keep the notch output zero and thus the interferometer in quadrature (:o.p.d. = $\frac{1}{4}\lambda$). This continuously ensures the maximum sensitivity of the interferometer. Further details about the stabilisation are given by Kwaaitaal¹ et al. The signal I_f is given at the bandpass output of selective amplifier 1. I_f has an amplitude \hat{I}_f and is detected by phase sensitive detector 1 (p.s.d.1) tuned to f .

Under these conditions a vibrational electrostrictive dilatation (with a frequency f and an amplitude $|(\Delta L_1)_f|$) of the sample is calculated to be⁴

$$(\Delta L_1)_f = \pm \left[2\pi(I_{\max} - I_{\min}) \right]^{-1} \lambda \hat{I}_f \quad (2)$$

The positive sign in (2) corresponds to an expanding sample.

We use disklike samples with a diameter of 5 mm.

The two flat and parallel surfaces of the disk are either evaporated with a gold layer or coated with silverpaint. Electrical contacts to

the electrodes on the sample are made by thin supple gold wires 3 cm long and 20 μm thick. These wires take care of the mechanical isolation between sample and the coax cable to the high voltage amplifier. This is important since Coulomb forces cause the coax cable to vibrate. Stray fields are kept at a minimum by the coax cable, the sample electrodes and the form of the sample. Any change in the relative positions of coax cable, sample and gold wires did not effect the measurements of electrostrictive dilatations. Therefore we conclude that the effect of stray fields may be neglected.

The sample and mirror are mounted on an orientable support. This is necessary for aligning the interferometer.

The whole interferometer is placed on a granite slab (0.9 x 0.9 x 0.08 m^3) with four air cushions underneath. This provides sufficient isolation from mechanical vibrations of the floor.

Electrostriction in the dielectric sample is generated by E_1 , an electric field provided by the high voltage amplifier connected to oscillator 1. E_1 consists of a d.c. field E_0 plus an a.c. field $\hat{E} \cos 2\pi f_0 t$ in which f_0 is the frequency set by oscillator 1. The high voltage amplifier supplied an AC voltage V_{f_0} superimposed on a DC voltage V_0 . Building up of space charges in the sample could complicate the calculation of E_1 . Therefore we estimated the RC-time of the samples. This was found to be in the order of minutes. We did not find any such time dependence in the measured electrostrictive dilatations. So E_1 is calculated in the usual simple way. The voltages V_{f_0} and V_0 have maxima of 450V r.m.s. and ca. 750V, respectively. To ensure approximately static conditions while retaining the advantages of a.c. detection, f_0 has been set between 30 and 200 Hz. Substituting $E_1 = E_0 + \hat{E} \cos 2\pi f_0 t$ in (1) gives

$$\Delta L_1 = (\Delta L_1)_{2f_0} \cos 4\pi f_0 t + (\Delta L_1)_{f_0} \cos 2\pi f_0 t + (\Delta L_1)_0$$

with

$$(\Delta L_1)_0 \equiv \gamma_{1111} (E_0^2 + \frac{1}{2} \tilde{E}^2) L_1$$

$$(\Delta L_1)_{f_0} \equiv 2\gamma_{1111} E_0 \tilde{E} L_1 \quad \text{and} \quad (3a)$$

$$(\Delta L_1)_{2f_0} \equiv \frac{1}{2} \gamma_{1111} \tilde{E}^2 L_1 \quad (3b)$$

The p.s.d. 1 uses oscillator 1 as a reference and is able to detect signals either at frequency f_0 or $2f_0$. Combining (2) with either (3a) or (3b) leads to an expression for γ_{1111} .

A calibrated dilatation is obtained by applying a signal with an amplitude $\hat{V}_{q,f}$ to a quartz crystal attached to mirror 2. This crystal has a known orientation and a well known piezoelectric constant² $d_{111} = -2.3 \times 10^{-12}$ m/V.

Oscillator 2 provides the frequency f of $\hat{V}_{q,f}$, that is either f_0 or $2f_0$, and is synchronised by the frequency coupler to oscillator 1. Coherent expanding and shrinking of this quartz crystal and the sample at the same amplitude is detected by p.s.d. 1, so that

$$(\Delta L_1)_f = \pm d_{111} \hat{V}_{q,f} \quad (4)$$

The sign in (4) is determined by a phase shift (0° or 180°) of the signal at the output of the frequency coupler. Zero phase shift corresponds to a shrinking sample and a positive sign in (4). Within the experimental error of 10% the results of (2) and (4) are the same for $(\Delta L_1)_f$.

A second harmonic distortion $\delta V_{2f_0} / V_{f_0}$ of the electrostatic amplifier leads to dilatations $\delta(\Delta L_1)_{2f_0}$ of piezoelectric samples.

This piezoelectric effect is reduced by at least a factor of 10 by using a sample in which two identically orientated piezoelectric crystals were set on top of each other. The outer electrodes of the disc-like crystals were grounded while the middle one was connected to the electrostatic amplifier. Measurements with the 100:1 attenuator, selective amplifier 2 and p.s.d. 2 showed that δV_{2f_0} was less than 6 mV. Thus, in a quartz crystal we have $\delta(\Delta L_1)_{2f_0} = d_{111} \delta V_{2f_0} / 10 < 2 \times 10^{-15}$ m. This value may be neglected in view of the sensitivity of this interferometer. In this instance $\delta V_{2f_0} / V_{f_0}$ was less than 0.002% in the measurements on quartz.

Results and discussion

In the literature, small values of γ_{ijkl} are theoretically predicted for diamond⁵ and have been measured on quartz^{6,7}. The information given about sign and magnitude of γ_{1111} , however, is inconclusive. We have therefore performed experiments on single crystals of these materials and on a single crystal of LiF which was used in electrostriction experiments by Bohaty⁸.

Quartz ($L_1 = 2.96$ mm, $\hat{E} = 1.43 \times 10^5$ V/m, Brasil quartz, x-cut) showed a value of γ_{1111} of $(-6 \pm 2) \times 10^{-22} \text{ m}^2/\text{V}^2$ which is surprisingly low compared with earlier data⁷ of $2.5 \times 10^{-20} \text{ m}^2/\text{V}^2$. However, they do not yield an analysis of second-harmonic distortion. Possibly the discrepancy may be inputted to this effect as rather stringent requirements of $\delta V_{2f_0} / V_{f_0}$ have to be met. Our value of γ_{1111} determined from (3b) is in good agreement with the value⁶ of γ_{3333} of $+3 \times 10^{-22} \text{ m}^2/\text{V}^2$.

Diamond ($L_1 = 0.50$ mm, $E_0 = 1.40 \times 10^6$ V/m, purest⁹ type II A) showed a value of γ_{1111} of $(+1.7 \pm 0.3) \times 10^{-22} \text{ m}^2/\text{V}^2$ which is about

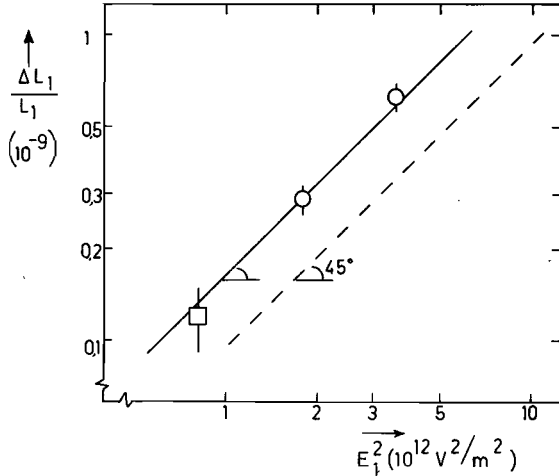


Fig. 2 The electrostrictive strain in diamond is given as a function of E^2 . The circles and square show the results (and their error) of the measurement of $(\Delta L_1)_{F_0}$ and $(\Delta L_1)_{2F_0}$, respectively. The electrostriction constant can be calculated according to (1). The broken line shows the theoretical prediction according to Maradudin⁵.

twice that of a theoretical prediction⁵ based on the values of the dielectric, elastic and elasto-optic constants of diamond. The experimental results of $(\Delta L_1)_{F_0}/L_1$ and $(\Delta L_1)_{2F_0}/L_1$ are marked in Fig. 2 by circles and a square, respectively, corresponding to $E_1^2 = 2E_0 \hat{E}$ (3a) and $E_1^2 = \frac{1}{2}\hat{E}^2$ (3b). This presentation allows γ_{1111} to be calculated according to (1).

Lithium fluoride ($L_1 = 3.00$ mm, $\hat{E} = 2.12 \times 10^5$ V/m) showed a value of γ_{1111} of $(-7.9 \pm 0.8) \times 10^{-21} \text{ m}^2/\text{V}^2$ which is in fair agreement with $(-7.2 \pm 1.1) \times 10^{-21} \text{ m}^2/\text{V}^2$ found by Bohatý⁸. γ_{1111} has been determined from (3b).

Two types of forces contribute to the value of γ_{1111} as defined in (1) i) Attracting Coulomb forces acting between the electrodes on the sample ii) Forces acting inside the sample itself, such as Coulomb forces between electric-field induced dipoles. The first effect has been described by Bohatý⁸. The second, much larger effect has been described by a model proposed by Luymes¹⁰. The experimentally found value of γ_{1111} is the result of these two effects.

Highest accuracy attainable is 10% and follows from the standard deviation of γ_{1111} measured at several frequencies. The sensitivity of the interferometer determines the final accuracy.

1. Th.Kwaaitaal, B.J.Luymes and G.A.van der Pijll, J.Phys.D 13, 1005 (1980).
2. J.F.Nye, Physical Properties of Crystals (Pergamon Press, Oxford, 1976).
3. M.Born and E.Wolf, Principles of Optics (Pergamon Press, London, 1959), p.258.
4. A.A.Fotchenkov, Sov.Phys. Crystallogr. 2, 653 (1957).
5. A.A.Maradudin, Phys.Rev. 164, 1081 (1967).
6. I.S.Zheludev, Physics of Crystalline Dielectrics (Plenum Press, New York, 1971), Vol. II, p.613.
7. J.J.Gagnepain and R.Besson in Physical Acoustics, edited by W.P.Mason (Academic Press, New York, 1975), Vol XI, p.245.
8. L.Bohatý and S.Haussühl, Acta Crystallogr. A, 33, 114 (1977).
9. Landolt-Börnstein: New Series, edited by O.Madelung (Springer-Verlag, Berlin, 1982), group III: Vol 17a, p.36.
10. B.J.Luymes, PhD Thesis, Eindhoven University of Technology, (1982).

2:2 Noise sources in the interferometer

Noise sources have a tendency to change sensitivity of the interferometer for the worse. They introduce real or imaginary vibrations. In general vibrations of a sample are described by the following equation¹⁶ (see section 2.1)

$$|(\Delta L_1)_f| = \lambda \hat{I}_f \left[2\pi(I_{\max} - I_{\min}) \right]^{-1} \quad (2.1)$$

$|(\Delta L_1)_f|$ is the amplitude of a vibrating sample at a frequency f . λ is the laserlight wavelength. \hat{I}_f is the amplitude of a current measured on the phase sensitive detector. This signal originates from the photodiode in the interferometer. I_{\max} and I_{\min} are the maximum and minimum current in the photodiode, respectively, corresponding to the maximum and minimum of the interference pattern projected on this photodiode.

Several noise sources influence the measurement of $|(\Delta L_1)_f|$. These sources are: laser noise, shot noise and excess noise in the photodiode, amplifier noise, mechanical noise, thermal fluctuations and acoustic noise, and refractive index noise.

The shot noise in the photodiode, caused by the photon character of light, sets the detection limit of this interferometer. This is explained in the article at the end of this section. It is experimentally verified in section 2.3.

Refractive index noise is caused by temperature variations along the laserbeampath in the interferometer. The refractive index n depends on the temperature T , roughly according to¹⁷ $\partial n / \partial T \approx 10^{-6} \text{K}^{-1}$. Changes in n cause variations in the optical path difference since

this is expressed as a number of wavelengths λ . This number, $\hat{I}_f \left[2\pi(I_{\max} - I_{\min}) \right]^{-1}$ determines $|(\Delta L_1)_f|$ according to (2.1). Therefore the refractive index noise causes a noise component $\Delta L'$ of $|(\Delta L_1)_f|$. This component is negligible under normal circumstances, when compared to the sensitivity of the interferometer.

The intensities of mechanical, thermal, acoustic and refractive index noise show an increase with an increasing optical path difference between the two branches of the interferometer¹⁸. According to (2.1) it follows that

$$\Delta \hat{I}_f = \frac{\partial \hat{I}_f}{\partial (L_2 - L_1)} \Delta(L_2 - L_1) + \frac{\partial \hat{I}_f}{\partial L'} \Delta L' + \frac{\partial \hat{I}_f}{\partial (I_{\max} - I_{\min})} \Delta(I_{\max} - I_{\min}) + \frac{\partial \hat{I}_f}{\partial \lambda} \Delta \lambda + \Delta \hat{I}_{f, \text{rest}} \quad (2.2)$$

Here $2(L_2 - L_1)$ is the optical path difference between the branches of the interferometer. It is influenced by displacements of interferometer parts. The optical path differences, induced by refractive index noise, are described by L' . The value of $I_{\max} - I_{\min}$ varies along with the quality and power of the interference pattern. The mode beating of the laser varies λ somewhat. $\Delta \hat{I}_{f, \text{rest}}$ includes all other sources. The quantity to be measured ΔL_1 has been left out in (2.2). Noise sources influence the parameters given in (2.2). This is shown in the table below. The table also shows when the occurrence of these sources is manifest.

Photodiode noise and amplifier noise are noises in the detecting system. They influence the measurement of \hat{I}_f . This influence can be treated as if they were noise components in \hat{I}_f .

The quantity $\Delta \hat{I}_f$ leads to the uncertainty in $(\Delta L_1)_f$ as seen by (2.1).

Table 2.1 The influence of noise sources upon the parameters given in (2.2).

	$L_2 - L_1$	L'	$(I_{\max} - I_{\min})$	λ	$\Delta I_{f,rest}$	occurrence
laser noise			x	x		warming up period
displacements:						
a) mechanical origin	x		x			touching the interferometer
b) acoustic origin	x		x			hand clapping
c) thermal expansion			x			continuously
refractive index noise		x				blowing across the laserbeam path
amplifier noise					x	continuously
shot- and excess noise in the photodiode					x	continuously

A detailed treatment of the shot noise mentioned in tabel 2.1 is given in the following article which has been published in the "Journal of Physics D: Applied Physics"⁷. Some of the other noise sources are also treated.

Noise limitations of Michelson laser interferometers

Th Kwaaitaal, BJ Luymes and GA van der Pijll
Eindhoven University of Technology, Department of Electrical Engineering,
Eindhoven, Netherlands

Received 1 October 1979, in final form 28 December 1979

Abstract. The noise limitations of two types of stabilised Michelson interferometers are analysed. These interferometers are suitable for the measurement of vibrational amplitudes in the picometre and femtometre range. Formulae are derived for the attainable signal-to-noise ratio, assuming that the shot noise of the photodiode sets the fundamental limitation. Measurements on several He-Ne lasers show that good agreement between theory and experiment is possible.

1. Introduction

Michelson interferometers can be used to measure vibrational amplitudes down to about 10^{-14} m and for this purpose it is necessary to stabilise the sensitivity. We will concern ourselves with two types of stabilised interferometers. The first is stabilised by means of an electronic control system, the second by a special optical arrangement. A brief description follows, based on detailed descriptions of both principles by Kwaaitaal (1974) and Vilkomerson (1976).

In the electronically stabilised interferometer, as shown in figure 1, an interference pattern is produced and its luminous intensity is detected by a photodiode. The sample length is varied by an AC signal. This variation is much less than the wavelength of the He-Ne laser light. The length variation gives an intensity variation which is detected by the photodiode. The sensitivity to this variation depends on the position in the curve of luminous intensity versus path length difference (figure 2). This position can be varied by the DC level shift on the piezoelectric path length modulator. This position will also vary as a result of temperature changes and acoustic perturbations. The information on the optimum position is derived from the mean current through the photodiode. Comparison with a reference current produces an error signal that can be filtered, amplified and fed to the path length modulator to effectively stabilise the luminous intensity at one point.

The principle of the optically stabilised interferometer is shown in figure 3. The $\lambda/8$ plate introduces an optical path length difference of $\lambda/4$ between two perpendicularly polarised components of the laser beam in one arm of the interferometer. The angle between the polarisation direction of the laser source and the optical axes of the $\lambda/8$ plate is 45° . This gives two interference patterns which are in quadrature of phase. These two patterns are separated by the polarising beam-splitter (a Wollaston prism) and detected by the two photodiodes. Due to the $\lambda/4$ phase shift in one polarisation direction the AC signals from the sample vibrations are $\pi/2$ out of phase in the photodiode currents. That means that one AC photodiode signal (x) is a sine function of

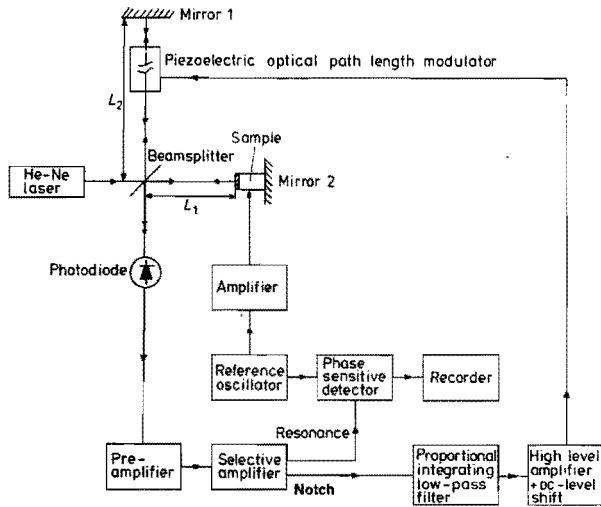


Figure 1. Schematic diagram of the electronically stabilised interferometer.

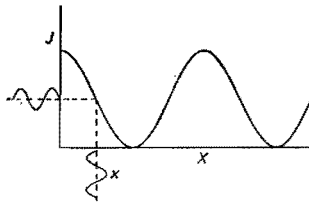


Figure 2. The dependence of the luminous intensity J on the mirror displacement X .

the variation of the mean path length difference while the other signal (y) exhibits a cosine-like variation.

This implies that the operation $z = (x^2 + y^2)^{1/2}$ leads to a constant sensitivity independent of the static optical path length difference. The arithmetical operation is performed by a vector computer which is part of the double lock-in analyser used in our experiments.

The signal-to-noise ratio of both interferometers is determined by a number of noise sources. We distinguish between the shot noise in the photodiode current, the electronic noise (thermal noise in resistors and excess noise in integrated circuits), the noise from mechanical origin and noise originating from the laser, like plasma noise and mode interference noise. It will be shown that shot noise sets the main limitation on the sensitivity. As a consequence the signal-to-noise ratio will be calculated on the assumption that shot noise is the main noise source.

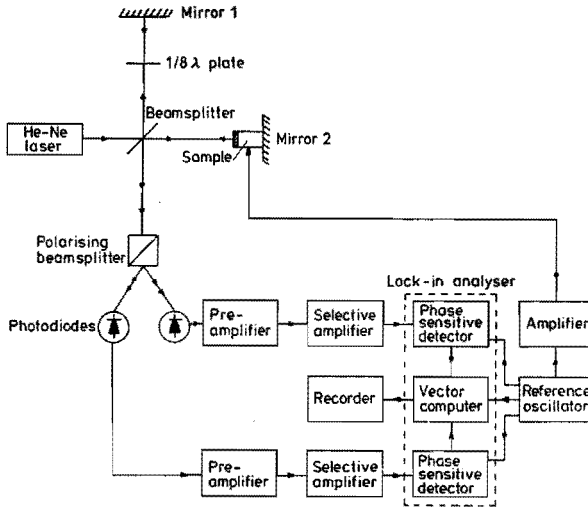


Figure 3. Schematic diagram of the optically stabilised interferometer.

2. Theory

Here we shall derive expressions for the signal-to-noise ratio. We assume that the separation of adjacent fringes in the interference pattern is much larger than the field of view, i.e. the diameter of the laser beam. This implies a low order of interference (Born and Wolf 1959) so that the light can be focused on the surface of the photodiode. This assumption can readily be confirmed experimentally.

The light, of power P , impinging on the photodiode can now be expressed as a function of the phase difference ϕ between the two arms of the interferometer (Born and Wolf 1959)

$$P = \frac{1}{2} \alpha P_0 (1 + C \sin \phi) \tag{1}$$

where P_0 is the power of the laser source in watts, α the attenuation factor of this laser power due to the reflections at the glass-air interfaces, etc. and C is a contrast factor accounting for the inequality of the power in the two arms. The factor $\frac{1}{2}$ is introduced because one half of the laser power is returned to the laser by the beam-splitter. In the general case of static and dynamic displacements of a mirror of the interferometer, we can write

$$\phi = [2(X + x)/\lambda] 2\pi \tag{2}$$

where X is a static and x a dynamic displacement of a mirror. The static displacement can also be expressed as the difference between the lengths L_1 and L_2 of the two arms of the interferometer from the light-separating surface of the beam-splitter to the surface of the reflecting mirrors. The optical path lengths of the two arms are $2L_1$ and $2L_2$. As it is of no consequence whether X is a multiple of $\lambda/2$ larger or smaller, within the above mentioned demand on the fringe separation we may write $X = L_2 - L_1 \pm n\lambda/2$.

If we confine ourselves to harmonic modulations of the sample displacement we can put

$$x = \hat{x} \sin 2\pi ft. \quad (3)$$

The photodiode current can be written as

$$\begin{aligned} I &= \frac{\eta q}{h\nu} P = \frac{\eta q}{h\nu} \frac{1}{2} \alpha P_0 \left(1 + C \sin \frac{4\pi}{\lambda} (X + x) \right) \\ &= \frac{\eta q}{h\nu} \frac{1}{2} \alpha P_0 \left(1 + C \sin \frac{4\pi X}{\lambda} \cos \frac{4\pi x}{\lambda} + C \cos \frac{4\pi X}{\lambda} \sin \frac{4\pi x}{\lambda} \right) \end{aligned} \quad (4)$$

where η is the quantum efficiency of the photodiode expressed as the number of electrons per photon; q is the charge of an electron, h is Planck's constant and ν is the frequency of the laser light. If $4\pi x/\lambda \ll 1$, thus for amplitudes smaller than about 1 nm, equation (4) reduces to

$$I = (\eta q/h\nu) \frac{1}{2} \alpha P_0 [1 + C \sin (4\pi X/\lambda) + (4\pi x/\lambda) C \cos (4\pi X/\lambda)]. \quad (5)$$

Starting from this expression we can calculate the signal-to-noise ratio for both types of interferometer assuming the shot noise of the photodiode to be the main noise source.

2.1. Electronically stabilised interferometer

In this case the information on the amplitude of the displacements I_s is contained in the third term of equation (5), i.e.

$$I_s = (\eta q/h\nu) \frac{1}{2} \alpha P_0 (4\pi x/\lambda) C \cos (4\pi X/\lambda). \quad (6)$$

The first and second terms of equation (5) determine the mean current $\langle I \rangle$ from which the shot noise is derived.

$$\langle i^2 \rangle = 2q \langle I \rangle \Delta f = 2q \Delta f (\eta q/h\nu) \frac{1}{2} \alpha P_0 [1 + C \sin (4\pi X/\lambda)] \quad (7)$$

where Δf is the bandwidth considered.

Now we can define the signal-to-noise ratio S/N as

$$S \triangleq (\langle I_s^2 \rangle / \langle i^2 \rangle)^{1/2} = \frac{2\pi \hat{x}}{\lambda} N_e^{1/2} \left(\frac{C^2 \cos^2 (4\pi X/\lambda)}{1 + C \sin (4\pi X/\lambda)} \right)^{1/2} \quad (8)$$

where $N_e = \eta \alpha P_0 / 2h\nu \Delta f$ is the number of electrons generated in the photodiode in the measuring time. The interpretation of this result is facilitated by figure 4, which gives the mean photodiode current $\langle I \rangle$ and the signal-to-noise ratio as a function of the displacement X . The signal-to-noise ratio turns out to be dependent on the position X in the interference pattern. By making the assumption that $4\pi x/\lambda \ll 1$, a singularity arises in the mathematical formula (8) at $X = 3\lambda/8$ if $C = 1$. This singularity has no physical meaning and disappears when Bessel function expansions are used in a more rigorous treatment. There is no need for such treatment, as in practice the contrast factor C is always less than unity.

2.2. Optically stabilised interferometer

In the case of the optically stabilised interferometer the signals on the two photodiodes are $\pi/2$ out of phase, thus for the one photodiode, the phase difference between the two beams, in accordance with equation (2) is

$$\phi_1 = (4\pi/\lambda)(X + x) \quad (9a)$$

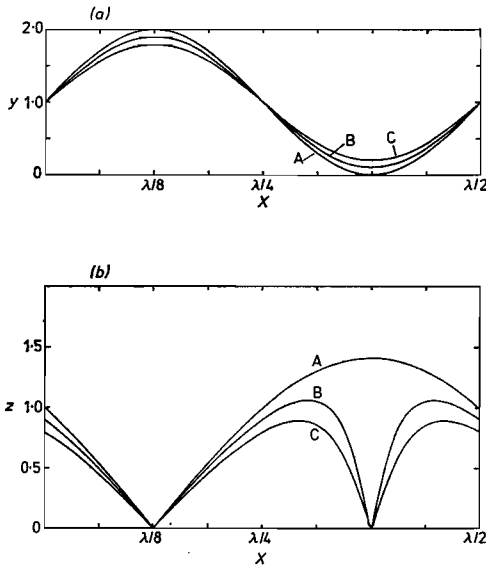


Figure 4. The mean photodiode current and signal-to-noise ratio as a function of path length difference from equations (5) and (8). (a) gives

$$y = \langle I \rangle / [(\eta q / h\nu) \frac{1}{2} \alpha P_0] = 1 + C \sin(4\pi X / \lambda)$$

and (b) gives

$$z = \frac{S/N}{(2\pi x / \lambda) N_e^{1/2}} = \left(\frac{C^2 \cos^2(4\pi X / \lambda)}{1 + C \sin(4\pi X / \lambda)} \right)^{1/2}$$

Curves A, B and C correspond to $C = 1.0, 0.9$ and 0.8 , respectively.

while for the other photodiode

$$\phi_2 = (4\pi / \lambda)(X + x) + \pi/2 = (4\pi / \lambda)[X + x + (\lambda/8)]. \tag{9b}$$

From this it follows that the currents I_1 and I_2 through photodiode 1 and 2 respectively are

$$I_1 = \frac{\eta q}{h\nu} \frac{1}{4} \alpha P_0 \left(1 + C \sin \frac{4\pi X}{\lambda} + \frac{4\pi x}{\lambda} C \cos \frac{4\pi X}{\lambda} \right) \tag{10a}$$

$$I_2 = \frac{\eta q}{h\nu} \frac{1}{4} \alpha P_0 \left(1 + C \cos \frac{4\pi X}{\lambda} - \frac{4\pi x}{\lambda} C \sin \frac{4\pi X}{\lambda} \right). \tag{10b}$$

The information signals I_{s1} and I_{s2} on photodiodes 1 and 2 respectively are

$$I_{s1} = (\eta q / h\nu) \frac{1}{4} \alpha P_0 (4\pi x / \lambda) C \cos(4\pi X / \lambda) \tag{11a}$$

$$I_{s2} = -(\eta q / h\nu) \frac{1}{4} \alpha P_0 (4\pi x / \lambda) C \sin(4\pi X / \lambda). \tag{11b}$$

The noise currents $\langle i_1^2 \rangle^{1/2}$ and $\langle i_2^2 \rangle^{1/2}$, generated in the two photodiodes are given by

$$\langle i_1^2 \rangle = 2q \langle I_1 \rangle \Delta f = 2q \Delta f \frac{\eta q}{h\nu} \frac{1}{4} \alpha P_0 \left(1 + C \sin \frac{4\pi X}{\lambda} \right) \quad (12a)$$

and

$$\langle i_2^2 \rangle = 2q \langle I_2 \rangle \Delta f = 2q \Delta f \frac{\eta q}{h\nu} \frac{1}{4} \alpha P_0 \left(1 + C \cos \frac{4\pi X}{\lambda} \right). \quad (12b)$$

To obtain a constant AC signal current independent of the displacement X , the operation $z = (x^2 + y^2)^{1/2}$ is performed on the two signal currents and thus on the two noise currents. We can therefore define a signal-to-noise ratio

$$S/N = \left(\frac{\langle I_{s1}^2 + I_{s2}^2 \rangle}{\langle i_1^2 + i_2^2 \rangle} \right)^{1/2} = \frac{\pi \bar{x}}{\lambda} N_e^{1/2} \left\{ C^2 \left[1 + \frac{1}{2} \sqrt{2} C \sin \left(\frac{4\pi X}{\lambda} + \frac{\pi}{4} \right) \right]^{-1} \right\}^{1/2}. \quad (13)$$

To interpret this result we plot in figure 5 the mean photodiode currents $\langle I_1 \rangle$ and $\langle I_2 \rangle$ and the signal-to-noise ratio as a function of the displacement X . From this figure

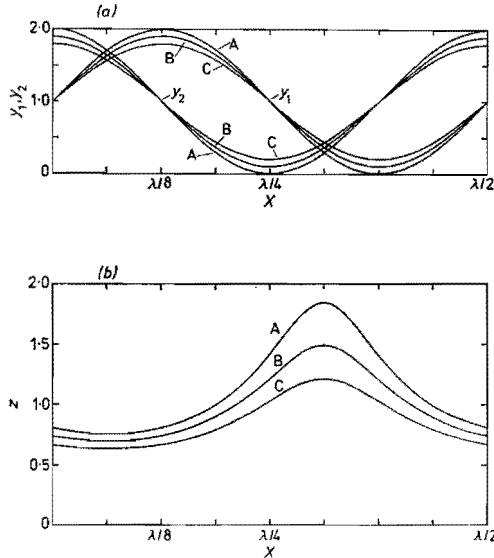


Figure 5. The mean photodiode current and signal-to-noise ratio as a function of path length difference from equations (10) and (13). (a) gives

$$y_1 = \langle I_1 \rangle / (\eta q / h\nu) \frac{1}{4} \alpha P_0 = 1 + C \sin (4\pi X / \lambda)$$

and

$$y_2 = \langle I_2 \rangle / (\eta q / h\nu) \frac{1}{4} \alpha P_0 = 1 + C \cos (4\pi X / \lambda)$$

and (b) gives

$$z = \frac{S/N}{(\pi \bar{x} / \lambda) N_e^{1/2}} = \left\{ C^2 \left[1 + \frac{1}{2} \sqrt{2} C \sin \left(\frac{4\pi X}{\lambda} + \frac{\pi}{4} \right) \right]^{-1} \right\}^{1/2}.$$

Curves A, B and C correspond to $C = 1.0, 0.9$ and 0.8 , respectively. Notice that the normalisation of S/N differs from that of figure 4 by a factor of two.

we see that the signal-to-noise ratio depends on the momentary value of the displacement X . If we take the contrast factor $C = 1$ we find for the maximum and minimum signal-to-noise ratio

$$(S/N)_{\max} = 1.8(\pi\hat{x}/\lambda)N_e^{1/2} \text{ at } 4\pi X/\lambda = 5\pi/4$$

and

$$(S/N)_{\min} = 0.77(\pi\hat{x}/\lambda)N_e^{1/2} \text{ at } 4\pi X/\lambda = \pi/4.$$

Comparison with the electronically stabilised interferometer having a theoretical maximum

$$(S/N)_{\max} = 2.8(\pi\hat{x}/\lambda)N_e^{1/2}$$

shows that the signal-to-noise ratio decreases, by a factor between two and four. The difference between the minimum and the maximum value inspired us to look for a solution in which the optically stabilised interferometer always operates in the point of the maximum signal-to-noise ratio. Electronic stabilisation in this point by using an extra modulating signal is a distinct possibility. Calculations show that this does not lead to an essential improvement with respect to the electronically stabilised interferometer (from §2.1). If electronic stabilisation is applied the operation $z = (x^2 + y^2)^{1/2}$ on the photodiodes is no longer essential. Subtracting the two photodiode signals (subtract because of opposition of phase) leads to

$$(S/N)_{\max} = 2.6(\pi\hat{x}/\lambda)N_e^{1/2}$$

if $C = 1$ and $4\pi X/\lambda = 5\pi/4$. The slight difference with the maximum signal-to-noise ratio of the electronically stabilised interferometer from §2.1 stems from the condition that $\phi_1 - \phi_2 = -\pi/2$.

It is interesting to make an estimate of the detection limit, i.e. of the value of \hat{x} corresponding to $S/N = 1$. We take a He-Ne laser with light of power $P_0 = 5$ mW at a wavelength $\lambda = 632.8$ nm, a photodiode with a quantum efficiency $\eta = 0.5$, and an optical system with a value of $\alpha = 0.1$. From these figures it follows that $N_e = 4 \times 10^{14}$. Using equation (8) and curve B in figure 4 we get for $C = 0.9$ and $X \approx 5\lambda/16$ and for a measuring bandwidth $\Delta f = 1$ Hz:

$$\hat{x} = 4.8 \times 10^{-15} \text{ m.}$$

3. Experiments and results

Some experiments were performed to confirm the assumption that the shot noise of the photodiode was the principal limitation to the detection limit. The noise spectra of (i) the electronic noise, (ii) the photodiode shot noise, (iii) the laser noise, (iv) the mechanical noise were determined.

The spectra are measured by means of the set-up shown in figure 6. The light from the laser source is detected by a photodiode (United Detector Technology type PIN 5D). The photodiode current i is converted in a voltage v by a current amplifier so that $v = iR_f$, where R_f is the feedback resistor. The signal and noise are measured by a Brookdeal lock-in analyser (type 9505) provided with a Noise Measurement Plug in Unit type 5049. A PAR model 189 selective amplifier is incorporated to prevent faulty measurements by overloading etc. As a reference signal an all purpose function generator (HP type 3312A) is used. The signal from the lock-in is recorded on an xt recorder.

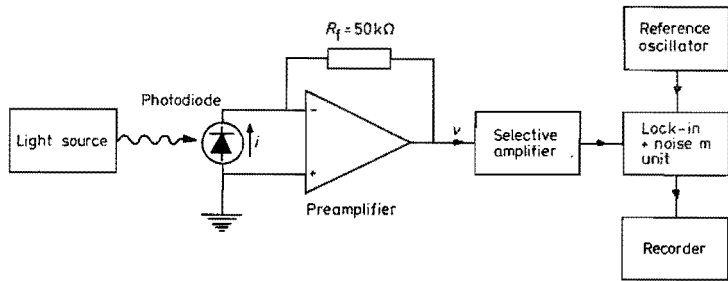


Figure 6. Schematic diagram of the set-up to measure noise spectra.

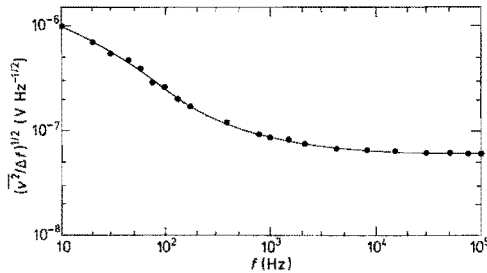


Figure 7. The noise spectrum of the photodiode and preamplifier. In the high frequency part of the spectrum the expected noise, $37 \times 10^{-9} \text{ V (Hz)}^{-1/2}$, is determined by the noise of the feedback resistor R_f and the noise of the operational amplifier.

(i) The noise spectrum of the photodiode and preamplifier is given in figure 7. At low frequencies excess noise caused a discrepancy between theory and experiments. The theoretical noise at higher frequencies is the sum of the thermal noise of the feedback resistor ($28.8 \times 10^{-9} \text{ V Hz}^{-1/2}$) and the noise of the IC amplifier ($23.7 \times 10^{-9} \text{ V Hz}^{-1/2}$) and thus equals $37 \times 10^{-9} \text{ V Hz}^{-1/2}$.

If the photodiode is not connected to the preamplifier a noise voltage of $36 \times 10^{-9} \text{ V Hz}^{-1/2}$, in excellent agreement with theory is measured. We have no explanation for the increase of the noise when the photodiode is connected. This point is, however, of minor importance compared to other noise sources, i.e. laser and shot noise.

(ii) The noise spectrum resulting from an incandescent lamp supplied from a DC source is given in figure 8. To obtain a normalised quantity independent of the luminous intensity of the source the squared noise voltage per Hz was divided by the voltage difference V_{11} at the output of the photodiode preamplifier corresponding with the light intensity. In the white part of the spectrum the agreement between measured and expected shot noise is excellent. The expected value in figure 8 is calculated using the shot noise formula

$$\langle i_n^2 \rangle = 2qI\Delta f$$

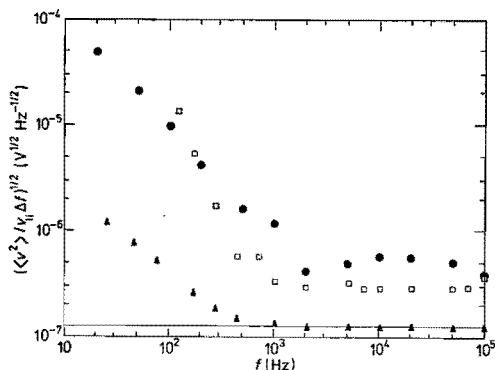


Figure 8. The normalised measured noise spectra of incandescent lamp (Δ), NEC laser (\square) and optically stabilised interferometer (\bullet). The solid line indicates the expected shot-noise level.

where $\langle i_n^2 \rangle$ is the effective value of the shot noise current squared, q the electronic charge, I the photodiode current and Δf the bandwidth of the measuring system. The contribution of the electronic circuitry is about 1% and thus negligible. This means that an interferometer with an incandescent lamp as a light source will show a sensitivity determined by the shot noise if the mechanical noise contribution can be neglected as discussed in §4. In the low frequency region below 1 kHz the spectrum is excess-noise dominated with an $f^{-1.7}$ dependence.

(iii) The analysis of the laser contribution to the total noise needs explanation. In literature (Levine and de Maria 1976) several noise contributions are mentioned with spontaneous emission noise giving the ultimate limit for the amplitude stability. In practice, certain externally controllable factors determine the attainable stability. These are mode interference, transition competition, plasma effects and environmental disturbances. The amplitude stability is also affected by irregularities and hum on the discharge current through the laser.

In multimode lasers, mode interference is a superposition of a swept frequency distorted sine wave on the mean laser intensity. The frequency varies between several kHz and 1–2 MHz. The duration of the sweep and its repetition rate depends on the temperature change of the plasma tube. If the laser has reached working temperature after a warming-up period and the environmental temperature is reasonably constant, the repetition rate may be as low as one sweep in ten minutes. As normal measurements can be made within one minute this noise source is of no importance, although its momentary amplitude is much higher (in the order of 20 dB or more than the other noise sources). In single-frequency lasers mode interference is absent.

Transition competition originates from the existence of several possible transitions in a He–Ne discharge. If one transition is selected by the choice of the Brewster window, this effect is unimportant.

Plasma effects include all discharge-induced perturbations that vary the population of the energy levels. It appears to be the most important noise source in the lasers examined. Radio frequency excitation is the best way to reduce this kind of noise.

This, however, introduces other problems, such as shortening the life of the laser tube, impedance matching problems and radiation effects. The three different types of spectra of plasma noise are given by Bellisio *et al* (1964). The first type is a spectrum with high noise in the 0–70 kHz region, and some excess noise above the photodiode shot noise at higher frequencies. A second type can occur with sharp spikes and apparently no excess noise between the spikes. The third spectrum is a flat spectrum that is shot-noise dominated. The occurrence of the first or second spectrum is determined by the discharge current amplitude, or by a capacitive loading of the discharge circuit. A transition between these two operations can always be effected. As the second spectrum shows no excess noise in the region between the spikes, appropriate choice of the frequency of the vibrational amplitudes will prevent plasma noise from influencing the signal-to-noise ratio.

Environmental disturbances include all external processes that alter the passive optical characteristics. They can be of thermal or mechanical origin. Owing to the rigid construction of our lasers this kind of noise is negligible.

We measured the noise spectra of five commercially available He–Ne lasers. Without special precautions, none of the lasers met the shot-noise limit set by the photodiodes over the entire frequency range. The spectra of the three multimode lasers had to be measured during time intervals in which no mode interference occurred. After thermal isolation, the Nippon Electric Company laser model GLG 2034 showed a spectrum which agreed well with the expected shot noise. The use of a well stabilised laser supply to get rid of hum would make reliable measurement of this spectrum possible in the range below about 1 kHz. This spectrum is shown in figure 8. One of the single-mode lasers also showed a spectrum that was mainly determined by shot noise in the high frequency range. Hum in the laser current prevented reliable measurement at frequencies below 10 kHz.

(iv) The noise spectrum of the optically stabilised interferometer is also given in figure 8. From equation (13) it follows that the signal-to-noise ratio has maxima and minima depending on the momentary value of the displacement X . As the minima correspond with a low light intensity and the maxima with a high light intensity, the applied normalisation of the noise brings both extremes in one point of the figure.

4. Discussion and conclusions

The noise spectra show that the signal-to-noise ratio decreases seriously at frequencies below 1 kHz due to excess noise. If we confine ourselves to frequencies from 1 kHz to 100 kHz the spectra show that the electronic noise is negligible at the light levels used in the experiments. These light levels correspond to photodiode currents in the order of 100 μ A. Furthermore it follows from figure 8 that a low noise laser meets the theoretical shot-noise limit to within a factor of two.

Figure 8 also shows that environmental noise does somewhat decrease the signal-to-noise ratio. This spectrum was measured in a quiet laboratory room during the day-time with closed doors and windows. This rather satisfactory result was reached by the rigid and compact construction of the interferometer. The spectrum of the electronically stabilised interferometer showed a similar behaviour.

As the influence of environmental noise can be reduced by proper acoustic isolation it is realistic to take the shot noise as the limiting factor for the sensitivity of the inter-

ferometer. If the application of the interferometer requires a constant and reliable detection limit it is necessary to avoid the mode beating effect and to use a single mode laser. The higher power of a multimode laser will increase the detection limit except during short periods at which the sensitivity is seriously decreased due to mode interference. The modulation frequencies must preferably be chosen above 1 kHz.

Acknowledgments

We thank Professor Dr F N Hooge for his valuable remarks on this subject. We are indebted to J L Cuypers for his accurate determination of noise spectra and to Ing W M M M van de Eijnden for his technical assistance.

References

- Bellisio J A, Freed C and Haus H A 1964 *Appl. Phys. Lett.* 4 5-6
- Born M and Wolf E 1959 *Principles of Optics* (Oxford: Pergamon Press)
- Kwaaitaal Th 1974 *Rev. Sci. Instrum.* 45 39-41
- Levine A K and de Maria A J 1976 *Lasers* Vol. 4 (New York: Marcel Dekker Inc.)
- Vilkomerson D 1976 *Appl. Phys. Lett.* 29 183-5

2:3 Detection limit of the interferometer

It would be very difficult to present an exact detection limit of the stabilized Michelson interferometer. It depends on factors as integrating time, frequency, laser power, several noise sources and loss factors which are discussed in⁷ section 2:2. A typical measurement involving very small vibrations is shown in fig. 2.1.

In fig. 2.1 a signal measured by phase sensitive detector 1 is shown before during and after the activation of a piezoelectric ceramic transducer with a signal of 1 μ V (r.m.s.). Calculations according to (2.1) showed a dilatation of 4.5 \pm 1fm (r.m.s.). The sensitivity of this transducer is 5.4 nm/V as determined from fig. 2.2.

The phase sensitive detector had an integrating time of 40 s. This corresponds with a sensitivity of 0.8 fm according to the calcu-

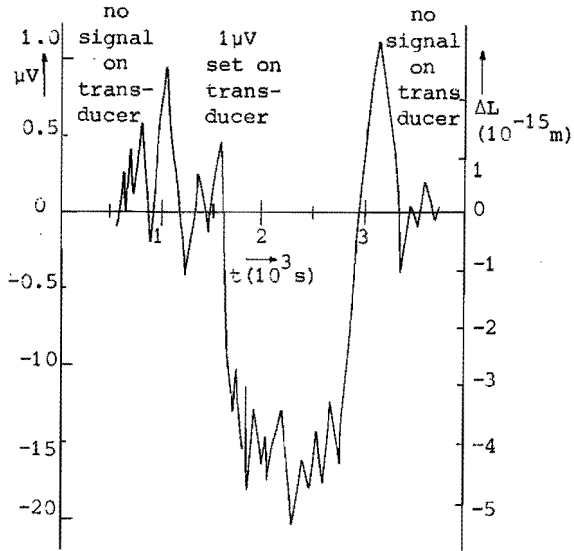


Fig. 2.1 Recorded signal from the phase sensitive detector 1 detecting a dilatation of $(4.5 \pm 1) \times 10^{-15}$ m on a piezoelectric ceramic transducer. On the right hand side the corresponding amplitude is presented.

lation given in section 2.1. This calculation uses the shot noise of the photodiode as the main limitation to the sensitivity of the interferometer. From figure 2.1 we can conclude that the noise on the signal has a peak-peak value of 2 fm and this is of the same order as the 0.8 fm mentioned above. The long measuring time of 1200 s is necessary to show the effect of the dilatation superimposed on the noise.

Figure 2.2 shows the linear relationship between the applied signal and the resulting dilatation in the piezoelectric ceramic transducer over seven decades.

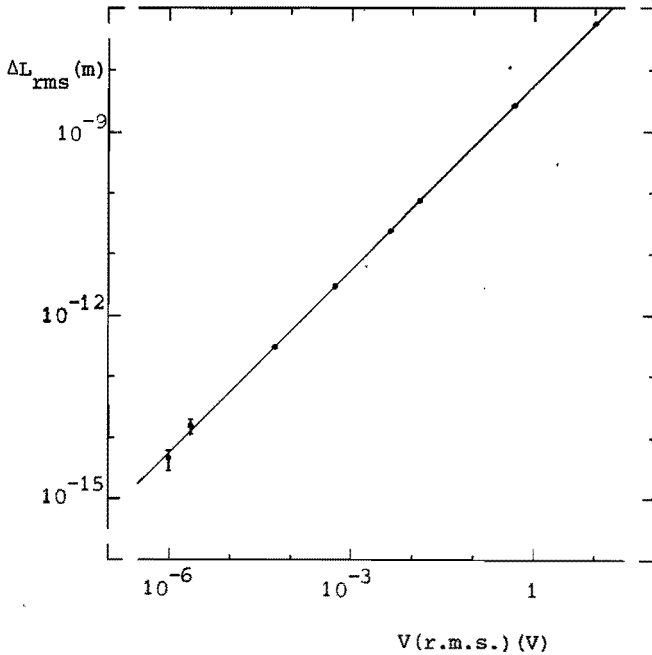


Fig. 2.2 The linear relationship between the voltage applied to a piezoelectric ceramic transducer and the corresponding dilatation. The sensitivity of the transducer is 5.4 nm/V.

The result shown in figure 2.1 is the one with the smallest dilatation shown in figure 2.2.

We may conclude that the measurements of ΔL are fundamentally limited by the shotnoise of the photodiode. Other noise sources play a minor role.

2:4 Reference dilatation

For the measurement of unknown electrostrictive dilatations of the order of 10^{-13} m it is important that calibrated dilatations are

available. They are used as references. Such a reference dilatation is created by applying a signal $V_{q,f}$ ($\approx 50\text{mV}$) to a specially selected piezoelectric crystal. Brasil, x-cut, quartz has a piezoelectric⁹ constant d_{111} of $-2.3 \times 10^{-12} \text{ m/V}$. This constant is independent of frequency below the resonant frequency ($\approx 10^5 \text{ Hz}$) of the quartz crystal. A crystal of this type has been attached to mirror 2 in the reference arm of the interferometer (see figure 1 in section 2.1). The signal $V_{q,f}$ is applied to this crystal by oscillator 2. The piezoelectric dilatation ΔL_f is determined using (2.1). The constant d_{111} can be determined from $\Delta L_f / V_{q,f}$. If this leads to $-2.45 \times 10^{-12} \text{ m/V} < d_{111} < -2.15 \times 10^{-12} \text{ m/V}$ the error in d_{111} is less than the total accuracy of 10% of this interferometer (see section 2.1). Larger errors than 10% can result from wrong tuning of the selective amplifiers with respect to the frequency of the oscillator which drives the quartz crystal. This can be easily corrected by retuning.

2:5 Contracting or expanding sample?

The stabilisation of the interferometer (section 2:1) locks the optical path difference to $\frac{1}{2}\lambda$ (disregarding multiples of $\frac{1}{2}\lambda$). The two possible points of stabilisation are shown in Figure 2:3.

One point is a stable point the other unstable. After activating the electronic stabilisation of the interferometer this stabilisation will lock the optical path difference in a stable point. Lets say this point is A, disregarding multiples of λ in the optical path difference. In A of A' the phase of a signal I_{f_0} resulting from

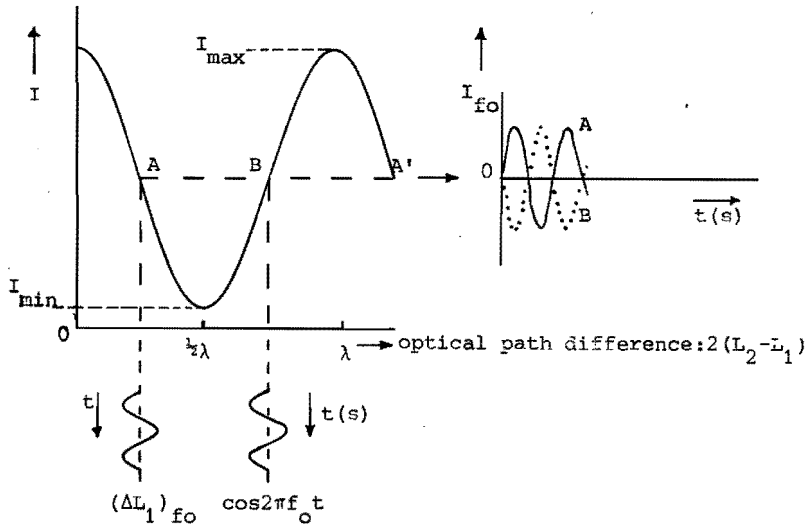


Fig. 2.3 The luminous intensity of the interference spot projected on the photodiode is either stabilised at point A or B. Dilatations $(\Delta L_1)_{f_0} \cos 2\pi f_0 t$ result in current changes I_{f_0} which are either in phase or 180° out of phase with the signal applied to the sample.

$(\Delta L_1)_{f_0} \cos 2\pi f_0 t$ will be the same. So the phase of I_{f_0} will never be changed by the stabilisation loop. This conclusion is also true if the stabilisation locks at point B.

As seen from figure 2.3 the phase of I_{f_0} gives no direct clue about the positive or negative value of $(\Delta L_1)_{f_0}$. Therefore we have to introduce a known dilatation and determine its corresponding phase.

A piezoelectric quartz crystal with a known orientation gives such a dilatation by applying an electric field to it.

According to Nye⁹ the following equations are true for a compressed x-cut quartz crystal

$$P_1 = d_{111} \sigma_{11} \quad (2.3)$$

where P_1 is the polarisation along the x-axis and σ_{11} the strain.

$$\Delta L_1/L_1 = d_{111} E_1 \quad (2.4)$$

It follows from (2.3) that P_1 indicates the positive x-axis since d_{111} and σ_{11} are both negative. The determination of P_1 is shown in the figures 2.4(a-c). An electric field E_1 in the direction of the positive x-axis will result in a negative value of $\Delta L_1/L_1$ according to (2.4).

This is shown in figures 2.4 (d,e).

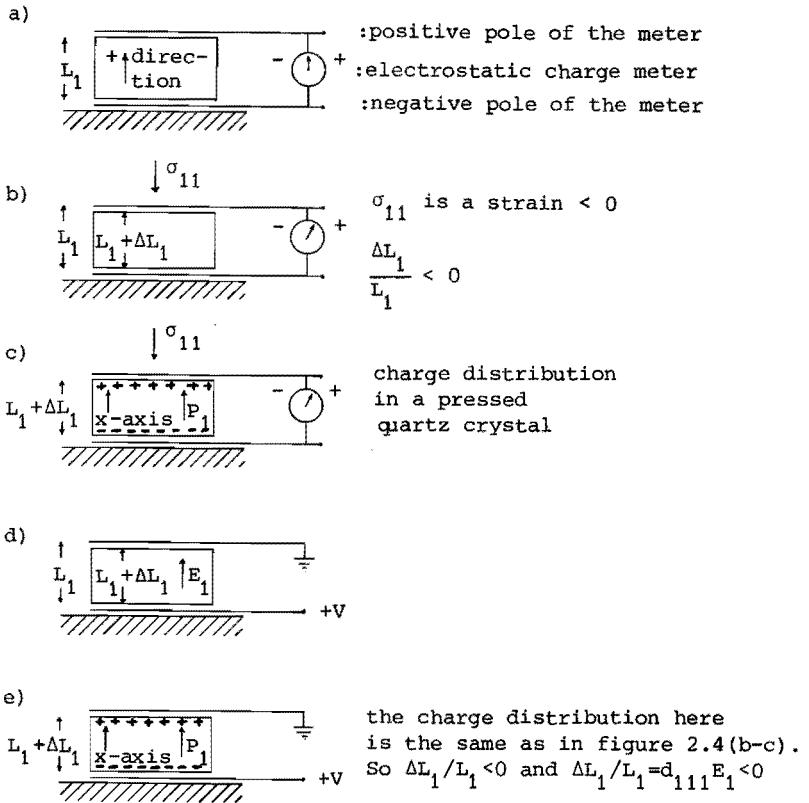


Fig. 2.4 A stress $\Delta L_1/L_1$ in a piezoelectric quartz crystal (x-cut) may be caused by a strain or an electric field. Comparing figures 2.4c and 2.4e with each other shows that an electric field E_1 , as shown above, will constrict the sample.

We use this knowledge in the following way. We measure the dilatation of a sample and detect the phase of I_{f_0} on the phase sensitive detector. We do not know whether this phase represents a contraction or an expansion of the sample. So we replace the sample by the contracting quartz crystal and measure the new phase. No difference between old and new phase implies that the sample contracts at "the same moment" as the quartz crystal. A 180° difference implies expansion at "the same moment". Once this is known the sign of an electrostriction constant is easily determined.

3 Theory of Electrostriction

3:1 An estimate of the electrostriction constant $|\gamma_{1111}|$

In order to estimate $|\gamma_{1111}|$ we assume that electrostriction is caused by electric-field-induced dipoles in the material to which the electric field has been applied. We also assume that without such a field there are no dipoles in the material.

The dipoles attract or repulse each other depending on their relative orientation. These dipoles cause stresses in the material which in turn cause strains.

First of all: What are the forces \vec{F} acting between two dipoles \vec{p}_1 and \vec{p}_2 ? For simplicity we assume that the dipoles are identical $|\vec{p}_1| = |\vec{p}_2| = p$. We determine \vec{F} in the following way.

The potential energy U_q of an electric charge q in the electric field of a dipole-moment p is given by the following potential

$$U_q(x,y) = \frac{pqx}{4\pi\epsilon_0(x^2+y^2)^{3/2}} = \frac{pq\cos\theta}{4\pi\epsilon_0 r^2} \quad (3.1)$$

where x , y , r and θ are shown in figure 3.1. ϵ_0 is the dielectric constant of vacuum and has been taken 8.8542×10^{-12} F/m. As will be seen further on we will only take into account nearest neighbour interactions between induced dipoles. Therefore it is justified to use just the dielectric constant of vacuum in (3.1).

We would like to know the potential energy U_p of a dipole \vec{p}_2 in the electric field of a dipole \vec{p}_1 . The force \vec{F} of \vec{p}_1 acting on \vec{p}_2 can be determined from

$$\vec{F}(x,y) = -\nabla U_p(x,y) \quad (3.2)$$

The force $F(x,y)$ depends in direction and strength on the relative

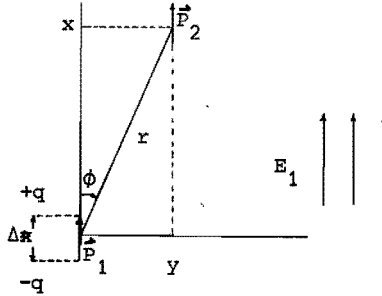


Figure 3.1 The relative position of two identical induced dipoles \vec{p}_1 and \vec{p}_2 in a material with an electric field E_1 applied to it. It is assumed that $\Delta x \ll r$

position of both dipoles.

In order to calculate $U_p(x,y)$ we define

$$p \equiv q\Delta x \quad , \quad \text{with} \quad \Delta x \ll r \quad (3.3)$$

We see from figure (3.1) that

$$\begin{aligned} U_p(x,y) &= U_q(x+\frac{1}{2}\Delta x, y) + U_{-q}(x-\frac{1}{2}\Delta x, y) = \\ &= U_q(x+\frac{1}{2}\Delta x, y) - U_q(x-\frac{1}{2}\Delta x, y) = \\ &= \left[\frac{\partial}{\partial x} U_q(x,y) \right] \Delta x \end{aligned} \quad (3.4)$$

Combining (3.1), (3.3) and (3.4) gives

$$U_p(x,y) = \frac{p^2}{4\pi\epsilon_0 (x^2+y^2)^{3/2}} \left(1 - \frac{3x^2}{x^2+y^2} \right) = \frac{p^2 (1-3\cos^2\theta)}{4\pi\epsilon_0 r^3} \quad (3.5)$$

Combining (3.2) and (3.5) gives

$$\vec{F}(x,y) = - \begin{pmatrix} \frac{\partial U_p(x,y)}{\partial x} \\ \frac{\partial U_p(x,y)}{\partial y} \end{pmatrix} = \frac{3p^2}{4\pi\epsilon_0 (x^2+y^2)^2} \begin{pmatrix} \frac{x}{(x^2+y^2)^{3/2}} \left(3 - \frac{5x^2}{x^2+y^2} \right) \\ \frac{y}{(x^2+y^2)^{3/2}} \left(1 - \frac{5x^2}{x^2+y^2} \right) \end{pmatrix} =$$

$$= \frac{3p^2}{4\pi\epsilon_0 r^4} \begin{pmatrix} \cos\theta(3-5\cos^2\theta) \\ \sin\theta(1-5\cos^2\theta) \end{pmatrix} = \vec{F}(r,\theta) \quad (3.6)$$

The direction of $\vec{F}(r,\theta)$ and its relative strength as a function of θ are shown in figures 3.2, 3.3 and table 3.1.

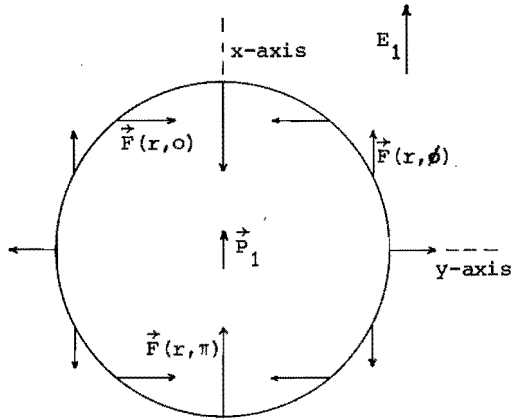


Figure 3.2 Direction and relative strength of forces $\vec{F}(r,\theta)$ acting between induced dipoles \vec{p}_1 and \vec{p}_2 . The origin of $\vec{F}(r,\theta)$ indicates the position of \vec{p}_2 on the circle. E_1 shows the direction of the electric field.

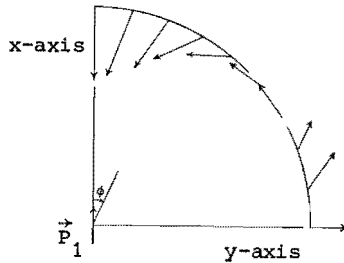


Figure 3.3 The forces $\vec{F}(r,\theta)$ acting on dipole \vec{p}_2 are shown in detail. $\vec{F}(r,\theta)$ has been calculated according to (3.6) and is tabulated in table 3.1.

θ	$(4\pi\epsilon_0 r^4/3p^2)\vec{F}(r,\theta)$	θ	$(4\pi\epsilon_0 r^4/3p^2)\vec{F}(r,\theta)$
0°	(-2.00, 0.00)	50°	(+0.60, -0.82)
10°	(-1.82, -0.67)	60°	(+0.88, -0.38)
15°	(-1.77, -0.95)	70°	(+0.83, +0.39)
20°	(-1.33, -1.17)	75°	(+0.69, +0.64)
30°	(-0.65, -1.38)	80°	(+0.49, +0.84)
40°	(+0.05, -1.24)	90°	(0.00, +1.00)
45°	(+0.35, -1.06)		

Table 3.1 Quantitative data derived from equation (3.6).

Figure 3.3 is based on these data.

The forces $\vec{F}(r,\theta)$ cause electrostrictive strains $\Delta L_1/L_1$ which will be estimated by using the next four assumptions

- 1) The electric-field-induced dipoles form a simple cubic lattice as seen in figure 3.4.
- 2) The strongest forces, $\vec{F}(r,0)$ and $\vec{F}(r,\pi)$, determine the strain σ_{11} . These forces can be seen in figure 3.2. We only take into account these forces if they result from nearest dipoles interaction.
- 3) The induced polarisation of the material is $P'_{11}E_1$. The volume reserved for one dipole is r^3 as seen in figure 3.4. Therefore

$$|\vec{P}_1| = p = r^3 P'_{11} E_1$$
- 4) Only the strain σ_{11} will be taken into account.

We describe the stress in the x direction as σ_{11} with

$$\sigma_{11} = -|\vec{F}(r,0)|/r^2 \quad (3.7)$$

Here we made use of the assumptions 1 and 2. Combining (3.6) and (3.7) gives

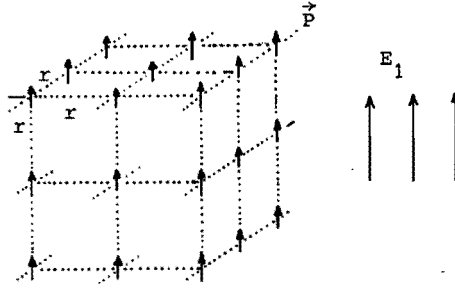


Figure 3.4 Simple cubic dipole lattice used to estimate $|\gamma_{1111}|$.

The dipoles p are induced by the electric field E_1 .

$$\sigma_{11} = -6p^2 / (4\pi\epsilon_0 r^6) \quad (3.8)$$

Using assumptions 3 and 4 together with the following equation for bulk material

$$\Delta L_1 / L_1 = S_{1111} \sigma_{11} + \dots$$

and neglecting other stresses, gives

$$\Delta L_1 / L_1 = -6S_{1111} p_{11}^2 E_1^2 / (4\pi\epsilon_0) \quad (3.9)$$

S_{ijkl} (m^2/N) is a component of the elastic compliance.

The above equation, together with the definition of electrostriction, leads to the following estimate for the electrostrictive constant

$$\gamma_{1111} = -6S_{1111} p_{11}^2 / (4\pi\epsilon_0) \quad (3.10)$$

In this simple model γ_{1111} can only be negative. However, the sign of γ_{1111} depends strongly on the goniometric factors included in $\vec{F}(r, \theta)$. If different dipole lattices are considered we will find different directions of $\vec{F}(r, \theta)$.

Such a change to another lattice could easily result in a positive value of γ_{1111} . An example of a positive γ_{1111} is given in chapter 6 for the diamond lattice. So (3.10) can only be used to estimate the order of magnitude of $|\gamma_{1111}|$.

We will now check if the assumption $\Delta x \ll r$ is right. The volume per dipole is r^3 as shown in figure 3.4. This may be considered as the volume of an atom of the material investigated for electrostriction. Since $r^3 = (10\text{\AA})^3$, $E_1 < 10^6 \text{V/m}$, $P'_{11} < 10^{-9} \text{F/m}$ and $q \approx 10^{-19} \text{C}$, combining (3.3) with the third assumption leads to

$$\Delta x < 10^{-11} \text{m} \ll r = 10^{-9} \text{m}$$

It follows that $\Delta x \ll r$ is a correct assumption.

The value of $|\gamma_{1111}|$ of several materials has been estimated with (3.10). The results are shown in table 3.2 together with the values of S_{iiii} and P'_{ii}/ϵ_0 which are used in the estimate. This table also shows the experimentally found value of γ_{iiii} . Figure 3.5 shows the good correlation between the estimated values and experimental values of $|\gamma_{iiii}|$. Index i refers to one or more specific crystallographic axes in the single crystal. The values of i are given in table 3.1.

We see that the estimate of $|\gamma_{iiii}|$ gives the correct order of magnitude. The result shown in (3.9) has the same form as (1.1):

$\Delta L_i/L_j = Q_{ijkl} P_k P_l$, if one remembers that $P'_{ij} E_j = P_i$. We conclude that (3.9) and (3.10) are realistic relations.

When we are interested in the temperature dependence of γ_{1111} we should first look at the temperature dependence of S_{1111} and P'_{11} . According to (3.10) this will give some information about γ_{1111} as a function of temperature.

In an analogous way we can look at γ_{ijkl} in general and see if there is any temperature dependence to expect.

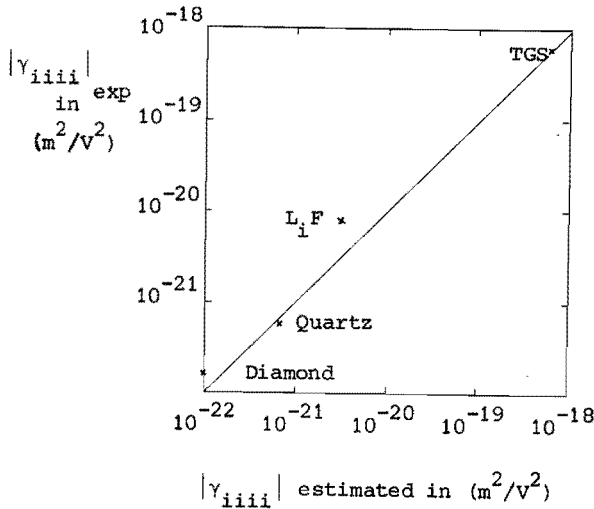


Figure 3.5 Experimental values of $|\gamma_{iiii}|$ versus the estimated values of $|\gamma_{iiii}|$. These estimates are made according to (3.10). Details about the value(s) of i are given in table 3.2.

For further empirical relations between electrostriction constant and other material constants we refer to Uchino and Cross²³.

Theoretical estimates of γ_{1111} in the alkali halogenides have been made by Grindlay and Wong³⁷. According to Bohatý²⁶ these estimates result in the same sign as the experimentally found value of γ_{1111} .

Apart from the electrostriction caused by internal forces in a sample between the electrical induced dipoles there is a smaller attractive Coulomb force between the electrodes of the sample. These forces result in an extra strain $-\frac{1}{2}S_{1111} \epsilon_r \epsilon_o$ according to Haussthl

et al²⁷. This correction has no influence on the order of magnitude of γ_{1111} which has been estimated in this section.

Table 3.2 Comparison of the theoretically estimated and experimentally observed values of γ_{iiii} .

	S_{iiii} ($10^{-12} \text{ m}^2/\text{N}$)	$P'_{ii}/\epsilon_0 = \epsilon_r - 1$	γ_{iiii} in $10^{-21} \text{ m}^2/\text{V}^2$	
			equation (3.10) absolute values	experimental
diamond ¹⁹ (i=1,2,3)	0.955	4.86	0.095	+0.17
quartz ⁹ (i=1)	12.7	3.5	0.66	-0.6
LiF ^{20,21} (i=1,2,3)	11.7	7.9	3.1	-7.9
Triglycine sulphate ²² (i=2)	70	44	570	-600

3:2 Relation between the dielectric constant and the electrostriction constant.

The relation between the stress dependence of the dielectric constant $\partial P'_{11}/\partial \sigma_{11}$ and γ_{1111} is calculated by Nye⁹. That calculation is repeated here.

Combining the first and second laws of thermodynamics results in

$$dU = \sigma_{ij} d(\Delta L_i/L_j) + E_i dD_i + TdS \quad (3.11)$$

U is the internal energy of a crystal, D_i is the dielectric displacement

and S the entropy. We now have to consider the free energy function ϕ defined by

$$\phi = U - \sigma_{ij} (\Delta L_i / L_j) - TS - ED \quad (3.12)$$

Combining (3.11) and (3.12) leads to

$$d\phi = -\Delta L_i / L_j d\sigma_{ij} - D_i dE_i - SdT \quad (3.13)$$

We see from (3.11) and (3.12) that ϕ is a function of σ_{ij} , E_i and T .

Hence we may write

$$d\phi = \left(\frac{\partial \phi}{\partial \sigma_{ij}} \right)_{E,T} d\sigma_{ij} + \left(\frac{\partial \phi}{\partial E_i} \right)_{\sigma,T} dE_i + \left(\frac{\partial \phi}{\partial T} \right)_{\sigma,E} dT \quad (3.14)$$

The suffixes indicate which variables have been kept constant in determining the differentials of ϕ . Comparing the coefficients of (3.13) and (3.14) gives

$$\left(\frac{\partial \phi}{\partial \sigma_{ij}} \right)_{E,T} = -\Delta L_i / L_j, \quad \left(\frac{\partial \phi}{\partial E_i} \right)_{\sigma,T} = -D_i \quad (3.15)$$

Differentiating the first equation of (3.15) with respect to E_k and the second with respect to σ_{ij} and after changing the indices from i to k gives

$$\left(\frac{\partial (\Delta L_i / L_j)}{\partial E_k} \right)_{\sigma,T} = \left(\frac{\partial D_k}{\partial \sigma_{ij}} \right)_{E,T} \quad (3.16)$$

Differentiating (3.16) with respect to E_l gives

$$\left(\frac{\partial^2 (\Delta L_i / L_j)}{\partial E_k \partial E_l} \right)_{\sigma,T} = \frac{\partial}{\partial \sigma_{ij}} \left(\frac{\partial D_k}{\partial E_l} \right) = \frac{\partial}{\partial \sigma_{ij}} \left(P'_{kl} \right) \quad (3.17)$$

Since

$$\gamma_{ijkl} = \frac{1}{2} \left(\frac{\partial^2 (\Delta L_i / L_j)}{\partial E_k \partial E_l} \right)_{\sigma, T}$$

the equation (3.17) results in

$$\gamma_{1111} = \frac{1}{2} \frac{\partial P'_{11}}{\partial \sigma_{11}} \quad (3.18)$$

The tensor component $\partial P'_{11} / \partial \sigma_{11}$ has not been measured directly since large homogeneous stresses are necessary to measure any change in P'_{11} in materials like diamond. It is possible, however, to apply a hydrostatic pressure σ . This has been done by Waxler and Weir¹⁵. They measured $\partial n_{11} / \partial \sigma$ where n_{11} is the refractive index. If we look at a fixed frequency, $n_{11}^2 = P'_{11} / \epsilon_0 + 1 = \epsilon_r$ by definition, where ϵ_r is the relative dielectric constant. It is then easily calculated that

$$\frac{\partial P'_{11}}{\partial \sigma_{11}} + \frac{\partial P'_{11}}{\partial \sigma_{22}} + \frac{\partial P'_{11}}{\partial \sigma_{33}} = -2n_{11} \epsilon_0 \frac{\partial n_{11}}{\partial \sigma} \quad (3.19)$$

The minus sign in (3.19) results from the fact that a hydrostatic pressure corresponds with compressive or negative stresses. The three terms on the left side of equation (3.19) will partly compensate each other. Assuming that the terms with σ_{22} and σ_{33} describe secondary effects, it follows that

$$\left| \frac{\partial P'_{11}}{\partial \sigma_{11}} \right| > \left| 2n_{11} \epsilon_0 \frac{\partial n_{11}}{\partial \sigma} \right| \quad (3.20)$$

Combining (3.18) and (3.20) results in

$$|\gamma_{1111}| > \left| n_{11} \epsilon_0 \frac{\partial n_{11}}{\partial \sigma} \right| \quad (3.21)$$

As seen in table 3.3 the absolute experimental value $|\gamma_{1111}|$ is indeed larger than $\left| n_{11} \epsilon_0 \frac{\partial n_{11}}{\partial \sigma} \right|$.

Table 3.3 Comparison between the experimental value of γ_{1111} and¹⁵
 $n_{11} \epsilon_0 \frac{\partial n_{11}}{\partial \sigma}$ as determined by (3.21)

	$\frac{\partial n_{11}}{\partial \sigma} (10^{-12} \text{ m}^2/\text{N})$	n_{11}	$\gamma_{1111} (10^{-21} \text{ m}^2/\text{V}^2)$	$-n_{11} \epsilon_0 \frac{\partial n_{11}}{\partial \sigma} (10^{-21} \text{ m}^2/\text{V}^2)$
diamond	-1.15	2.418	+0.17	+0.025
quartz	+10.9	1.55	-0.6	-0.15
LiF	0	1.392	-7.9	0

Details about table 3.3 will be discussed in the chapters 5 to 8 dealing with the individual crystals.

4 Electrostriction in practice

4:1 Sample requirements

We like to compare theory with experiments. Therefore we chose materials with well-known properties which can be (partly) described by well-known relations. At the end of this section some details about these relations are given.

The sensitivity, 10^{-13} m, of the stabilized Michelson interferometer can be used in two ways.

- 1) ELECTROSTRICTIVE CONSTANTS, as small as $10^{-22} \text{ m}^2/\text{V}^2$, can be measured. This requires the use of high electric fields, 10^6 V/m , in order to get a detectable dilatation.
- 2) LOW ELECTRIC FIELDS, 10^4 V/m , can be used in measurements of large electrostrictive constants, $10^{-18} \text{ m}^2/\text{V}^2$.

The last mentioned method is important in piezoelectric materials, where second-harmonic distortion of the applied voltage causes dilatations which can easily be confused with electrostrictive dilatations. If only low electric fields are required the second-harmonic distortion will be a small percentage of the applied voltage.

The experimental layout of the interferometer²⁴ permitted the use of solid samples with a diameter up to 5 mm.

We used dielectric materials. In these materials, electric fields in the range of 10^4 to 10^6 V/m will not cause any warming-up. Therefore we can use a simple, no power delivering, high voltage amplifier. Single crystals of known orientation are required. We used LiF, diamond, quartz and triglycine sulphate. These crystals will be discussed in detail in chapters 5, 6, 7 and 8 respectively.

4:2 Details on the preparation and mounting of the sample

A conductive layer on the flat sides of the disclike samples provided the necessary electrodes on the sample. The layer was made of silverpaint or by evaporating gold or silver. The second method sometimes had the advantage that the evaporated layer could also be used as a mirror. We generally preferred the silverpaint electrodes. The necessary mirror was then easily stuck to the sample.

Electrical connections to the sample were made of gold wires. They were attached to the sample by silverpaint. Great care had to be taken to avoid an electrical short-circuit by spilling some silverpaint on the sides of the sample which had a thickness of only 1mm.

The orientation of the crystals was checked by the Laue back reflection method²⁵.

The sample had to be fixed to a support with two degrees of freedom. This enabled the alignment of the laserbeam of the interferometer.

The sample was attached to a partly rotateble support by using grease as an "adhesive". This was necessary in order to let the sample move freely. The influence of a rigid support on the induced strains of a sample is discussed in chapter 7. The crystal had to be mounted horizontally on the support in order to prevent a deteriorating of the interference pattern caused by slipping away. This is seen in figure 4.1. An example of the sample preparation is given in figure 5.1.

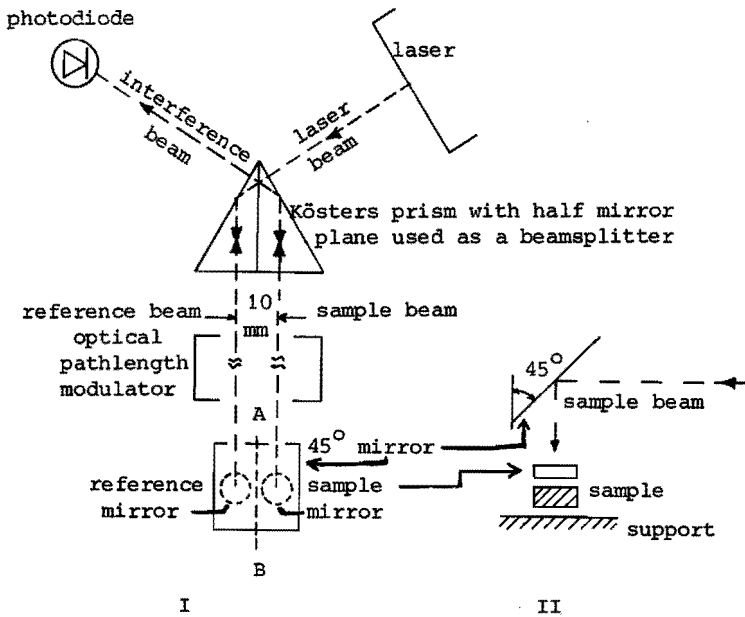


Figure 4.1 I Topview of the arrangement of the stabilized Michelson interferometer. AB is the plane of symmetry between reference and sample beam. Actually the sample and reference mirror cannot be seen underneath the 45° mirror.

II A partly rotatable support fixed on the common background of reference and sample mirror.

4:3 Experimental difficulties in measuring true electrostrictive dilatations.

The stabilized Michelson interferometer is isolated from outside mechanical vibrations by fixing it on a rigid slab of granite. This slab rests in turn on four air-filled tires. The effects of mechanical vibrations that still come through are reduced in three ways.

- 1) The reference- and sample-beam of the interferometer are kept

as near to each other as possible. In this case 10 mm as shown in figure 4.1.

- 2) The lightpaths of the interferometer are kept as short as possible. They are about 20 cm.
- 3) The random lightpath variations between sample-and reference-beam are compensated by the electronic stabilisation described in detail by Kwaaitaal²⁴.

The electronic stabilisation compensates random variations. However, there is one exception: vibrations, having the same frequency as the electrostrictive dilatations of the sample. This frequency is $2f_0$ and is the second harmonic of the frequency f_0 of the voltage V_{f_0} which is applied to the sample.

There are four sources of signals at $2f_0$ which are detected by the phase sensitive detector. One source is the sinusoidal form of the interference relation. This will be discussed in section 4.4. Another source is the second harmonic distortion of the high voltage amplifier connected to a piezoelectric sample. This will be discussed in chapter 7.

The remaining sources of vibrations with frequency $2f_0$ will be discussed below. They are caused by Coulomb interactions.

I : A Coulomb interaction between electric charges q can be described by a force F with

$$F \sim q^2 \sim (C_s V_{f_0})^2 ; V_{f_0} \sim E_0 + \hat{E} \cos 2\pi f_0 t \quad (4.1)$$

C_s is a stray capacitance of the electrical contacts leading to the sample. It follows from (4.1) that F has frequency components at f_0 and $2f_0$. The Coulomb interaction causes vibrations at $2f_0$ of the electrical contacts on the sample and thus of the sample itself. The intensity of these vibrations is linear with $V_{f_0}^2$. Therefore these vibrations

look very much like electrostrictive vibrations. So they have to be reduced. This has been done in four ways.

- 1) The electrical contacts are shielded, until very near the sample. This reduces F between cable and surroundings.
- 2) The actual electrical contacts on the sample are made of 20 μm thin supple gold wires. This reduces the mechanical coupling between the wires and the sample.
- 3) The electrical contacts are laid symmetrical with respect to the supports of reference- and sample-beam mirrors. (The plane of symmetry is indicated by the line AB in figure 4.1). In this way any vibration of the common support of the mirrors will have the same influence on the position of these mirrors. Simultaneous movement of both mirrors is not detected in this interferometer.
- 4) A mechanical resonance frequency of $2f_o$ of some part of the equipment near the sample will alter the phase of the signal measured on the phase sensitive detector. We are glad for this phase change since this provides the criterium with which we circumvent resonance vibrations. To prevent such a resonance, one has to vary f_o in order to find the signal with the right phase when compared with V_{f_o} . An example of a positive electrostrictive dilatation ΔL_1 is given as a function of time, together with V_{f_o} , in figure 4.2.

The frequencies we used lay in the range of 30 to 200 Hz. This corresponds to the "quiet" region given by Bohatý²⁶.

II: A Coulomb force also acts between the electrodes stuck to the sample. This force results in a strain $(\Delta L_1/L_1)_C$ given by Haussühl and Waldu²⁷

$$(\Delta L_1/L_1)_C = -\frac{1}{2} S_{1111} \epsilon_r \epsilon_o V_{f_o}^2 / L_1^2 \quad (4.2)$$

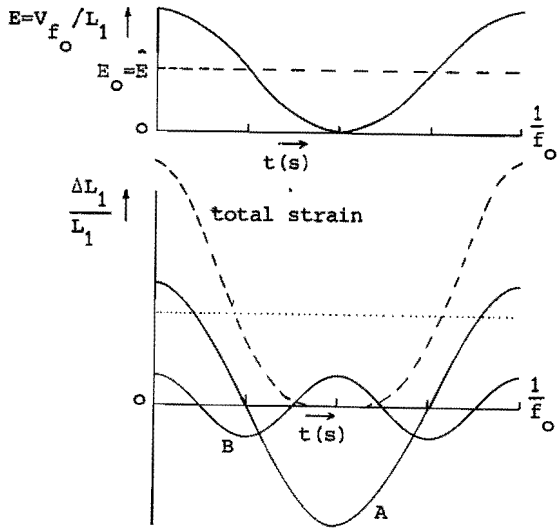


Figure 4.2 The electric field applied to the sample is shown above.

The lower part shows the three frequency components of the electrostrictive strain with $(\Delta L_1)_f / L_1 = \gamma_{1111} (E_0^2 + \frac{1}{2} E^2)$; dotted line $(\Delta L_1)_f / L_1 = 2\gamma_{1111} E_0^2$; curve A and $(\Delta L_1)_{2f} / L_1 = 4\gamma_{1111} E^2$; curve B. The broken line shows the sum of these three components.

Estimating the electrostrictive strain $(\Delta L_1 / L_1)_c$ is easy. If $(\Delta L / L)_c$ would be the only effect contributing to electrostriction of the sample, we would measure a value of γ_{1111} for diamond, quartz, LiF and triglycine sulphate of -0.025, -0.25, -0.46, $-1.4 \times 10^{-21} \text{ m}^2 / \text{V}^2$, respectively. This follows from (4.2) and the numerical data given in table 3.2. The results are of the order of the uncertainty in the measurement of the electrostrictive strains.

Only repeated measurements, under slightly different arrangements of the electrical contacts to the sample, can show if true electro-

strictive dilatations are measured. The electrostrictive dilatations have to vary linearly with $1/L_1$ if V_{f_0} is kept constant. This follows directly from the definition of electrostriction.

Another indication is the correct phase.

4.4 Non linearities introduced by the sinusoidal character of the interference relation.

The stabilisation of the luminous intensity $J(x)$ of the interference spot on the photodiode will not always keep $J(x)$ at $\frac{1}{2}(J_{\max} + J_{\min})$. Figure 4.3 shows $J(x)$, versus x , together with J_{\max} and J_{\min} . The level $\frac{1}{2}(J_{\max} + J_{\min})$ is the most sensitive part of the interference spot with respect to small dilatations (see chapter 2). Some change in the quality of the interference pattern may cause stabilisation at a level $\frac{1}{2}(J_{\max} + J_{\min}) + J_0$. Figure 4.3 shows J_0 with $J_0 \ll \frac{1}{2}(J_{\max} - J_{\min})$.

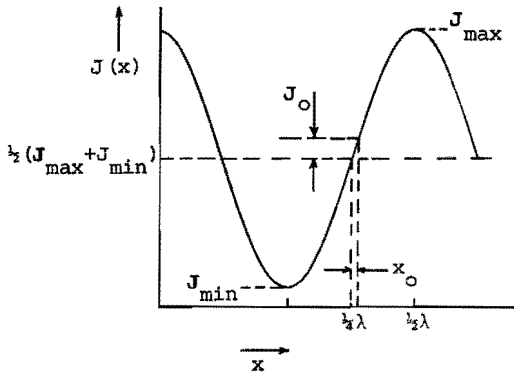


Figure 4.3 The luminous intensity $J(x)$ is shown as a function of the displacement x of the sample mirror. The level $\frac{1}{2}(J_{\max} + J_{\min})$ is the ideal stabilisation level. This level has no second-harmonic distortion caused by the sinusoidal character of J .

Now we will give a definition about the quality of the interference pattern.

The interference pattern is formed by the two interfering laserbeams of the interferometer. These beams have a luminous intensity of J_1 and J_2 (W) respectively. Under total interfering conditions $J_{\max} - J_{\min}$ is given by²⁸

$$(J_{\max} - J_{\min}) = 4\sqrt{J_1 \cdot J_2} \quad (4.3)$$

In practice $(J_{\max} - J_{\min}) < 4\sqrt{J_1 \cdot J_2}$. This is caused by not totally overlapping laserbeams at the interference place. The quality of the interference pattern may now be defined by $(J_{\max} - J_{\min}) / (4\sqrt{J_1 \cdot J_2})$. This value lay somewhere between 0.90 and 0.95 in our interferometer.

Now we will show that a stabilisation at $\frac{1}{2}(J_{\max} + J_{\min}) + J_0$ results in non-linearities in the measurement of small dilatations. They look like spurious dilatations $\left[(\Delta L_i)_{2f_0} \right]_{sp}$.

The function $J(x)$ is given by²⁸ the following equation

$$J(x) = \frac{1}{2}(J_{\max} + J_{\min}) + \frac{1}{2}(J_{\max} - J_{\min}) \cos 4\pi x / \lambda \quad (4.4)$$

We will make a Taylor expansion of $J(x)$ in powers of the displacement $(\Delta L_i)_{f_0} \sin 2\pi f_0 t$ around $x = (3/8)\lambda + x_0$. We define x_0 implicitly by the following relation $\sin(4\pi x_0 / \lambda) = 2J_0 / (J_{\max} - J_{\min})$. Figure 4.3 shows x_0 .

It follows from (4.4) that

$$J(3\lambda/8 + x_0 + (\Delta L_i)_{f_0}) = \frac{1}{2}(J_{\max} + J_{\min}) + J_0 + J_{f_0} \sin 2\pi f_0 t - J_{2f_0} \cos 4\pi f_0 t$$

with

$$(\Delta L_i)_{f_0} = \frac{\lambda J_{f_0}}{2\pi(J_{\max} - J_{\min})} \quad \text{and} \quad (4.5)$$

$$J_{2f_0} = J_0 J_{f_0}^2 / (J_{\max} - J_{\min})^2 \quad (4.6)$$

In the same way as $(\Delta L_1)_{f_0}$ has been defined in (4.5) we now define

$[(\Delta L_1)_{2f_0}]_{sp}$ by the following relation

$$\left[(\Delta L_1)_{2f_0} \right]_{sp} = \frac{\lambda J_{2f_0}}{2\pi (J_{\max} - J_{\min})}$$

Using (4.5) and (4.6) leads to

$$\left[(\Delta L_1)_{2f_0} \right]_{sp} = (\Delta L_1)_{f_0} \cdot \frac{J_0}{(J_{\max} - J_{\min})} \cdot 2\pi \cdot \frac{(\Delta L_1)_{f_0}}{\lambda} \quad (4.7)$$

with $\lambda = 6328\text{\AA}$.

The importance of $[(\Delta L_1)_{2f_0}]_{sp}$ will be shown in the following example.

We apply a voltage V_s to a piezoelectric sample. This results in a vibration with an amplitude $|(\Delta L_1)_{f_0}|$ of 10\AA . If the stabilization is not at its optimum the value of $J_0 / (J_{\max} - J_{\min})$ may be as high as 0.01. According to (4.7) this results in an spurious quadratic vibration with an amplitude of 10^{-3}\AA . Hence, when we measure such small quadratic vibrations, we have to check according to (4.7) if they can possibly result from spurious dilatations. This check is only needed in the case of piezoelectric materials where $(\Delta L_1)_{f_0}$ could be "large".

5 Electrostriction in LiF

The first measurements of electrostriction with our interferometer were done on a single crystal of lithium fluoride. This crystal was put at our disposal by Bohatý. He had determined the electrostriction constants of several alkali halogenides⁴ such as LiF and NaCl. His measurements had been performed with a capacitive dilatometer and resulted in electrostriction constants γ_{1111} of LiF and NaCl of (-7.2 ± 1.1) and $(6.7 \pm 1.0) \times 10^{-21} \text{ m}^2/\text{V}^2$, respectively. The negative value of γ_{1111} of NaCl was in contradiction with the positive value given by Zheludev¹². So there was some question about the sign of γ_{1111} in these materials.

We cut several samples of LiF out of the original sample of Bohatý. A sample is shown in figure 5.1. We applied grease to fix the sample to the support and mirror. First we used silverpaint but this resulted in an aging effect in the measurements of γ_{1111} . This was caused by the hardening of the silverpaint. This hardening restricted the movement of the sample through clamping by ca. 30%. This type of clamping will be discussed in detail in chapter 7.

We measured the linear striction $(\Delta L_1)_{f_0}$ and the quadratic striction $(\Delta L_1)_{2f_0}$. They are given by (3a) and (3b) in section 2.1.

$$(\Delta L_1)_{f_0} = 2\gamma_{1111} E_0 \hat{E} L_1$$

and

$$(\Delta L_1)_{2f_0} = \frac{1}{2} \gamma_{1111} E_0^2 L_1$$

where E_0 is the pooling field and \hat{E} is the amplitude of an a.c. field superimposed on E_0 (see figure 4.2). The values of $(\Delta L_1)_{f_0}$ and $(\Delta L_1)_{2f_0}$ were negative. They were determined according to the method described in chapter 2. This resulted in a value of γ_{1111} of LiF of

$(-7.9 \pm 0.8) \times 10^{-21} \text{ m}^2/\text{V}^2$. The results are in good agreement with the earlier one's on the same crystal $(-7.2 \pm 1.1) \times 10^{-21} \text{ m}^2/\text{V}^2$.

The hydrostatic pressure derivative of the refractive index $\partial n/\partial \sigma$ of LiF has been measured by Waxler¹⁵ to be zero. According to section 3.2 this suggests a very small electrostriction constant. However this was not found experimentally. The value of γ_{1111} is easily measured in different ways.

As seen in section 3.1 the dielectric constant is an important parameter in finding the right order of magnitude of γ_{1111} . The relative dielectric constant ϵ_r of LiF is 8.9 at low frequencies²¹. The refractive index n_{11} for a wavelength of 5875.62 Å in LiF is 1.392 (table 3.3). From this it follows that at light frequencies $\epsilon_r = n_{11}^2 = 1.94$. This shows that ϵ_r changes strongly with frequency. This change is caused by the ionic polarisation of LiF which only plays a role at low frequencies. The different values of the two frequencies used in the determinations of γ_{1111} and $n\partial n/\partial \sigma$ may cause the above mentioned discrepancy between the results for $n_{11}\epsilon_r\partial n_{11}/\partial \sigma$ and γ_{1111} in LiF.

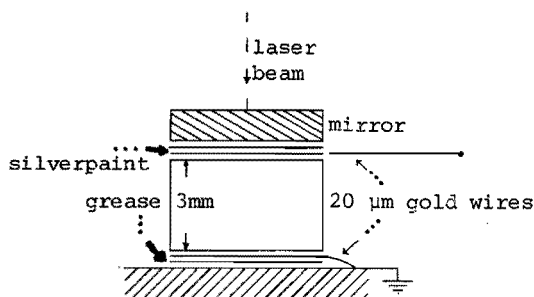


Figure 5.1 Sample of LiF with a diameter of 5 mm.

The electrostriction measured was of the order of 10^{-12} m .

6 Electrostriction in diamond

6.1 Information on the diamond samples

We distinguish four types of natural diamond¹⁹. The properties of these types are described in the table below.

Table 6.1 The properties of the four types of diamond.

Type	I		II	
	a	b	a	b
u.v. absorption range	$\lambda < 340\text{nm}$		$\lambda < 225\text{nm}$	
i.r. absorption range	$2.5\mu\text{m} < \lambda < 10\mu\text{m}$		$2.5\mu\text{m} < \lambda < 6\mu\text{m}$	
dark resistivity	$> 10^{14}\Omega\text{m}$		$> 10^{14}\Omega\text{m}$	$< 10^4\Omega\text{m}$
nitrogen content	500...2000 ppm	50...500ppm	<50 ppm	<50 ppm

We are interested in high resistivity and a low impurity contents so that the crystal can be submitted to electric fields of 10^6V/m or more. Therefore we have chosen the type IIa diamond. This type of diamond could be commercially obtained. Two diamond single crystal cylinders with a diameter of 5 mm are obtained from D. Drukker & Zn. N.V. (Amsterdam). The heights of these cylinders were 0.50 and 1.00 mm. They were prepared for the electrostriction experiments by evaporating gold mirrors on the flat surfaces of the cylinder. These mirrors also provided the necessary electrodes. Further details about the preparation are given in section 4.2.

The orientation of the cylinder axis was [100]. This was checked by an X-ray photo made with the Laue back-reflection method²⁵.

The structure of diamond is shown in figure 6.1. Each C-atom

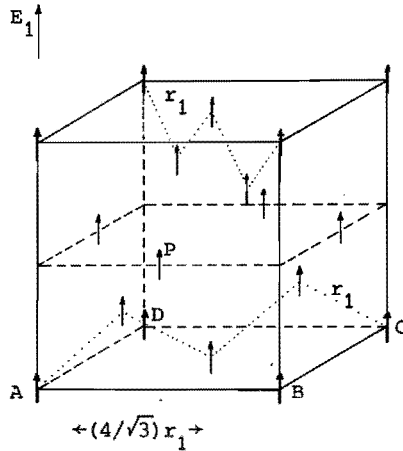


Figure 6.1 Positions of electric field induced dipoles p in a diamond lattice. E_1 indicates the direction of the electric field. r_1 is the nearest neighbour distance.

has four nearest neighbours. The distance between a C-atom and its nearest neighbours is 1.54449 \AA . The sides of the cube shown in figure 6.1 are $^{19} 3.56684 \text{ \AA}$ which is $4/\sqrt{3}$ times the nearest neighbour distance r_1 .

It is possible to estimate roughly the electrostriction in diamond along the lines given in section 3.1. But now we will take into account the actual crystal structure of diamond.

The calculation is given in the following section.

6:2 Estimate of γ_{1111} , using the crystal structure

The immediate surrounding of a C-atom in the diamond structure is given in figure 6.2. Only nearest neighbours are shown.

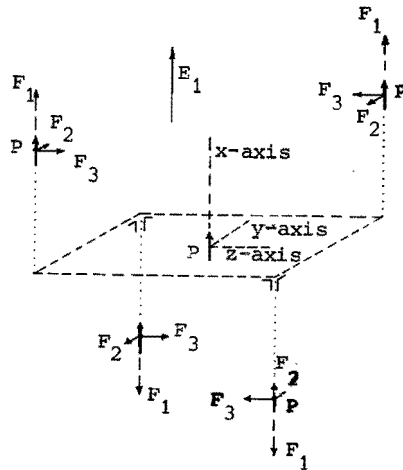


Figure 6.2 An induced dipole p in diamond with its four nearest neighbours. The forces of the central dipole acting on the nearest neighbour dipoles are shown. E_1 indicates the direction of the electric field.

The electric field applied to the diamond is along the x-axis. This field induces on each C-atom an identical dipole-moment p .

According to (3.6) dipole-dipole forces are linearly related to r^{-4} , where r is the distance between two dipoles. Forces between next-nearest neighbours will be neglected. The net result of these forces is nearly an order of magnitude smaller than nearest forces.

The force of a central dipole acting on a parallel dipole is given by (3.6). This equation is written in the new coordinates of figure 6.2.

$$\vec{F}(x,y,z) = \frac{3p^2}{4\pi\epsilon_0 r^4} \begin{pmatrix} \cos\theta(3-5\cos^2\theta) \\ \frac{1}{2}\sqrt{2}\sin\theta(1-5\cos^2\theta) \\ \frac{1}{2}\sqrt{2}\sin\theta(1-5\cos^2\theta) \end{pmatrix} = \begin{pmatrix} F_1 \\ F_2 \\ F_3 \end{pmatrix} \quad (6.1)$$

$$\text{with } \cos\theta = \frac{x}{r} = \frac{x}{(x^2+y^2+z^2)^{\frac{1}{2}}}$$

We had to change coordinates in order to let the new coordinates coincide with the crystallographic axes of diamond. The change involved a 45° turn around the x-axis. Hence the original y-component of $\vec{F}(x,y)$ in (3.6) is split up in the new y- and z-components given in (6.1).

In the case of diamond $|\cos\theta| = \sqrt{1/3}$ as is seen from figure 6.1. Using (6.1) results in

$$|F_1| = \frac{\sqrt{1/3} p^2}{\pi\epsilon_0 r^4} = 2|F_2| = 2|F_3| \quad (6.2)$$

The direction of the forces of the central dipole on the nearest dipoles is shown in figure 6.2.

Figure 6.1 shows that C-atoms in the ground plane ABCD (:a (100)-plane) have two nearest neighbours. In a (100)-plane there are two C-atoms in an area of $\frac{16r_1^2}{3}$. Now the stress σ_{11} between the ground plane and the parallel plane (at a distance $3^{-\frac{1}{2}}r_1$) above can be calculated. The same stress can be found for each pair of planes parallel to ABCD and at a distance of $3^{-\frac{1}{2}}r_1$ from each other. Therefore this stress exists in the whole crystal. The stress σ_{11} is calculated from (6.1) and (6.2).

$$\sigma_{11} = \frac{4|F_1|}{(16/3)r_1^2} \frac{\sqrt{3} p^2}{4\pi\epsilon_0 r_1^6} = -2\sigma_{22} = -2\sigma_{33} \quad (6.3)$$

In (6.3) we have calculated σ_{22} and σ_{33} along the same lines of reasoning

as σ_{11} . A negative stress means a compressive stress in the crystal.

The elastic stresses result in strains. We will calculate $\Delta L_1/L_1$ according to the next equation⁹

$$\Delta L_1/L_1 = S_{1111} \sigma_{11}$$

The above equation together with (6.3) results in

$$\frac{\Delta L_1}{L_1} = \sqrt{3} (S_{1111} - S_{1122}) p^2 / (4 \pi \epsilon_0 r_1^6) \quad (6.4)$$

with $S_{1122} = S_{1133}$.

In order to find $\Delta L_1/L_1$ we calculate p through the following relation

$$p = \frac{1}{8} \left(\frac{4}{\sqrt{3}} r_1 \right)^3 P'_{11} E_1 = \frac{8}{9} \sqrt{3} r_1^3 P'_{11} E_1 \quad (6.5)$$

where $P'_{11} E_1$ is the dipole moment per unit of volume, $(4/\sqrt{3} r_1)^3$ is the volume of the cube shown in figure 6.1 and the factor 1/8 stems from the fact that there are 8 C-atoms in the cube.

Combining (6.4) and (6.5) results in

$$\frac{\Delta L_1}{L_1} = \frac{16 \sqrt{3}}{27 \pi \epsilon_0} (S_{1111} - S_{1122}) P_{11}^2 E_1^2 \quad (6.6)$$

If we look at the definition of electrostriction it follows from (6.6)

that

$$\gamma_{1111} = +16 \sqrt{3} P_{11}^2 (S_{1111} - S_{1122}) / (27 \pi \epsilon_0) \quad (6.7)$$

The following values have experimentally been found for the material properties¹⁹ of diamond.

$$S_{1111} = 9.55 \times 10^{-13} \text{ m}^2/\text{N}$$

$$S_{1122} = -0.99 \times 10^{-13} \text{ m}^2/\text{N}$$

$$P'_{11}/\epsilon_0 = 4.86$$

If then follows from (6.7) that $\gamma_{1111} = 0.07 \times 10^{-21} \text{ m}^2/\text{V}^2$. We see

that this more realistic estimate results in the correct sign of the electrostriction constant. The rough estimate of section 3.1 always yields a negative sign. Taking into account 2nd nearest neighbours in the diamond structure only results in an increase of γ_{1111} of 13%. So γ_{1111} becomes $0.08 \times 10^{-21} \frac{m^2}{V^2}$.

6:3 Relation between γ_{1111} and the photo elastic constants

Maradudin and Burnstein³⁰ have found the electrostriction of diamond by using the tensor $(\gamma_{ijkl})_{cl}$. We will summarize their treatment. $(\gamma_{ijkl})_{cl}$ is defined implicitly by the following relation for a clamped sample

$$\sigma_{ij} = -\frac{1}{2}(\gamma_{klij})_{cl} E_k E_l$$

The suffix cl refers to the totally clamped condition of the sample. The tensor $(\gamma_{ijkl})_{cl}$ has the dimension of the dielectric constant of vacuum ϵ_0 . In diamond the tensor $(\gamma_{ijkl})_{cl}$ has three non-zero components. These are

$$(\gamma_{1111})_{cl} = P'_{11} + \partial P'_{11} / \partial (\Delta L_1 / L_1) \quad (6.8)$$

$$(\gamma_{1122})_{cl} = P'_{11} + \partial P'_{11} / \partial (\Delta L_2 / L_2) \quad (6.9)$$

$$(\gamma_{1212})_{cl} = \partial P'_{12} / \partial (\Delta L_2 / L_2)$$

The equations (6.8) and (6.9) together with

$$\gamma_{1111} = \frac{1}{2} S_{11ij} (\gamma_{11ij})_{cl}$$

lead to

$$\begin{aligned} \gamma_{1111} = & ({}^2S_{1111} + S_{1122})P'_{11} + {}^2S_{1111} \partial P'_{11} / \partial (\Delta L_1 / L_1) \\ & + S_{1122} \partial P'_{11} / \partial (\Delta L_2 / L_2) \end{aligned} \quad (6.10)$$

Here we see again a relationship between γ_{1111} and the tensors P'_{ij} and S_{ijkl} . The tensor $\partial P'_{ij} / \partial (\Delta L_k / L_k)$ can be easily derived from the photo elastic tensor $\partial (1/\epsilon_r) / \partial (\Delta L_i / L_i)$. The experimental values of $\partial (1/\epsilon_r) / \partial (\Delta L_1 / L_1)$ and $\partial (1/\epsilon_r) / \partial (\Delta L_2 / L_2)$ are given by³⁰.

$$\partial \left(\frac{1}{\epsilon_r} \right) / \partial (\Delta L_1 / L_1) = -0.49 \quad ; \quad (-0.244)$$

$$\partial \left(\frac{1}{\epsilon_r} \right) / \partial (\Delta L_2 / L_2) = +0.20 \quad ; \quad (+0.042)$$

The values of the other tensor components were already given in section 6.2. Using these values in (6.10) gives an estimate of γ_{1111} in diamond of $+0.093 \times 10^{-21} \text{ m}^2 / \text{V}^2$. The values between brackets are given by Landolt-Börnstein¹⁹. They lead to an estimated value of γ_{1111} of $+0.053 \times 10^{-21} \text{ m}^2 / \text{V}^2$.

All estimates lead to a positive value of γ_{1111} in diamond.

6:4 Measurement and conclusions

We applied a 450 V r.m.s. signal to a 0.50 mm thick diamond sample.

The electric field was parallel to one of the [100]-axes of diamond. The frequencies of the signals were chosen at 38,67 and 81 Hz. We detected an electrostrictive dilatation $|(\Delta L_1)_{2f_0}|$ equal to 63 fm ($=63 \times 10^{-15} \text{ m}$) at all three frequencies. $|(\Delta L_1)_{2f_0}|$ was found according to (2.1). The value of $(\Delta L_1)_{2f_0}$ is shown by point D in figure 6.3.

The problem is now whether the measured value of $|(\Delta L_1)_{2f_0}|$ corres-

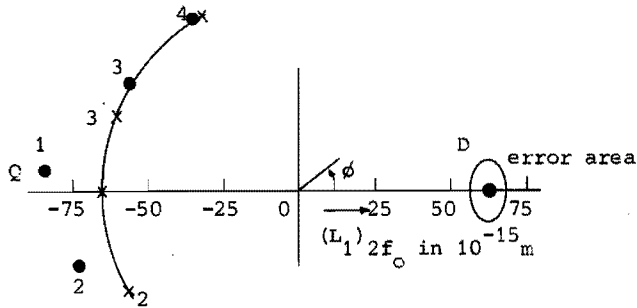


Figure 6.3 The compressive dilatation of a quartz crystal (Q) has a measured phase ϕ which is almost opposite to the measured phase of the electrostrictive dilatation of diamond (D). The crosses indicate calculated phase and amplitude of a quartz dilatation. The dots are the actually measured phase and amplitude.

ponded to an expansion or compression of the diamond during electrostriction. To solve this problem we introduced a compressive dilatation on a quartz crystal with known orientation. We applied a 0.020 V r.m.s. signal to the quartz crystal with a piezoelectric constant⁹ of -2.3×10^{-12} m/V. The expected value of -65 fm for the amplitude of the compressive dilatation of the quartz crystal is indicated by a cross with index 1 in figure 6.3. We measured a phase and amplitude on the phase sensitive detector which is represented by point Q in figure 6.3. We see that point Q has the opposite phase when compared to the electrostriction of diamond indicated by D. This means that the electrostriction in diamond corresponds to an expansion, so the γ_{1111} of diamond is positive.

To illustrate the errors involved in determining the γ_{1111} of diamond we vary the phase of the signal applied to the quartz crystal. The calculated amplitudes and phases are indicated by the crosses in figure 6.3, the dots represent the measured points. Corresponding crosses and dots have the same number. The difference between the crosses

and the dots gives an idea about the errors involved. Actually the error in $(\Delta L_1)_{2f_0}$ of diamond is estimated at 5 fm. We estimated this from the recording of the signal on the phase sensitive detector. An example of a recording is given in figure 2.1.

We used (3a) and (3b) of section 2.1 to calculate γ_{1111} . These equations are rewritten here

$$\gamma_{1111} = \frac{1}{2}(\Delta L_1)_{f_0} / (L_1 \hat{E} E_0) \quad (6.10)$$

$$\gamma_{1111} = 2(\Delta L_1)_{2f_0} / (L_1 \hat{E}^2) \quad (6.11)$$

The values of $(\Delta L_1)_{f_0}$, $(\Delta L_1)_{2f_0}$, \hat{E} and E_0 are given in the table below. We have also given the value of γ_{1111} calculated according to either (6.10) or (6.11). We recollect that $L_1 = 0.50$ mm.

Table 6.2 Numerical values used to calculate γ_{1111} of diamond according to either (6.10) or (6.11).

\hat{E} (10^6 V/m)	E_0 (10^6 V/m)	$(\Delta L_1)_{f_0}$ (10^{-15} m)	$(\Delta L_1)_{2f_0}$ (10^{-15} m)	γ (10^{21} m ² /V ²)
1.27	-	-	63 ± 5	$+0.16 \pm 0.02$
1.27	1.41	313 ± 15	-	$+0.18$
0.631	1.41	143 ± 12	-	$+0.16$

Figure 2 of section 2.1 can be made with the data in table 6.2. The experimental result for γ_{1111} is $(+0.17 \pm 0.03) \times 10^{-21}$ m²/V².

In the table below we will summarize the results given in several sections of this thesis.

Table 6.3 Summary of the estimates of γ_{1111} for diamond and the only experimental value of γ_{1111} .

estimates of γ_{1111} in $10^{-21} \text{ m}^2/\text{V}^2$ according to:			
section 3.1	:	+ 0.095	section 6.2 : + 0.07
section 3.2	:	> 0.025	section 6.3 : + 0.093; 0.053
experimental value of $\gamma_{1111} = + 0.17 \times 10^{-21} \text{ m}^2/\text{V}^2$			

We conclude that the experimental γ_{1111} is about twice or three times the estimated values. The sign of the experimental γ_{1111} is correct. No attempt will be made to explain the discrepancy of a factor 2 or 3.

7 Electrostriction in quartz

Before measuring the electrostriction in quartz we had to investigate two effects. These effects were (i) the clamping of the sample by the support and (ii) the piezoelectric dilatation of the quartz crystal caused by the unavoidable second-harmonic distortion in the electric field applied to the sample. These effects are discussed in section 7.1 and 7.2, respectively.

7:1 Clamping of the sample by the support

The effect of clamping is described in detail in the following article.³¹ To avoid this effect we used grease to fix the sample to the support.

Journal of Magnetism and Magnetic Materials 26 (1982) 187-190
North-Holland Publishing Company

CALCULATION AND MEASUREMENT OF MAGNETOSTRICTIVE CONSTANTS OF THIN LAYERS

Th. KWAAITAAL, B.J. LUYMES and W.M.M.M. van den EIJDEN

Eindhoven University of Technology, Department of Electrical Engineering, 5612 AE Eindhoven, The Netherlands

The striction of a disc-like sample clamped by a support is described by computer simulations as a function of the thickness-to-width ratio of the sample. Denting of the support has been taken into account. Experiments on quartz have shown that the support restricts the piezoelectric strain in two ways.

1. Introduction

We have analysed a problem related to the magnetostriction of thin samples. The magnetostrictive constant of a material is defined as the change in the dimensions of a material caused by magnetization, assuming the material expands freely. If the magnetostriction of thin samples is

measured, the last-named condition cannot always be fulfilled and it will be necessary to take into account the influence on the sample by clamping to the substrate or support. We met this problem for example when measuring the magnetostriction of aluminium-substituted nickel ferrites [1] where the largest dimensions of the crystal were between 1 and 2 mm. We measured the magnetostriction with a stabilized Michelson interferometer [2], capable of measuring vibrational amplitudes as small as 10^{-14} m, corresponding to strictions λ of the order of 10^{-8} in samples with a thickness of $1 \mu\text{m}$. To prevent undesired sample vibrations it has to be fixed rigidly to the interferometer.

As a suitable configuration of the samples, both for calculations and experiments, we have chosen a circular cylinder as shown in fig. 1a, which is attached to its support by a layer of glue. In the case of layers on a substrate, the thickness of the layer of glue is diminished and it is given the same properties as the support.

All calculations are made for isotropic materials. The finite-element method [3] was used to calculate, with the aid of a computer, the axial and tangential strains of the samples as a function of the dimensions of sample and glue and of the elastic properties of the sample, glue and support. A typical example of the deformation is shown in fig. 1b. The displacements are highly exaggerated. The deformation is caused by the restriction of the transverse strains of the sample by the support. These strains always accompany the axial strain of the mechanically free sample and, when these strains are reduced, so is the axial strain.

We made use of a computer simulation to calculate the mechanical clamping of thin samples or films by a support. The results of these calculations will be described in detail in sections 2, 3 and

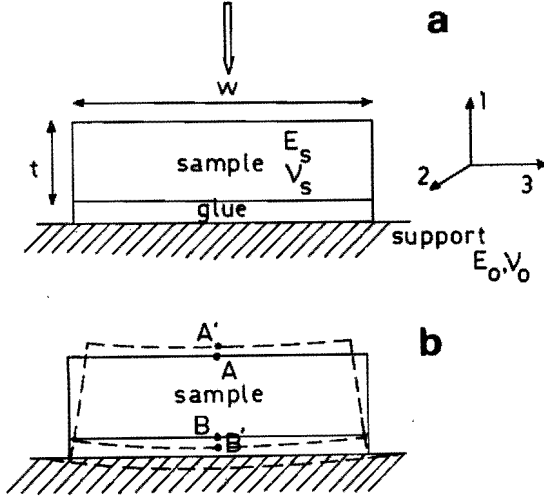


Fig. 1. (a) The configuration of the sample, glue and support, Young's moduli and Poisson's ratio of sample and support are indicated by E_s , ν_s and E_0 , ν_0 , respectively. The interferometer measures dilatations in the direction indicated by the large arrow. (b) A typical deformation (dotted) of a sample glued on to a support. The displacements are highly exaggerated.

4 and compared with experimental results in section 5.

2. Computer simulation

The configuration of sample and support used for the computer simulations is shown in fig. 1a. We will use the following terms in describing the influence of the support upon the movement of point A shown in fig. 1b: λ_f is the axial striction of the free sample. $\lambda_s(t/w)$ is the mechanically clamped striction of the sample which is principally a function of the thickness-to-width ratio t/w and is equal to $(A'B' - AB)/AB$, shown in fig. 2. ν is the Poisson's ratio; E is the Young's modulus; $\lambda_m(t/w)$ is the normalized movement of A which is experimentally easy to measure and equals AA'/AB shown in fig. 1b; $\lambda_0(t/w)$ is the normalized denting of the support shown as BB'/AB in fig. 1b; $\eta = \lambda_s(t/w)/\lambda_f$ and $\delta = \lambda_0(0)/\lambda_s(0)$.

A simple measurement of $\lambda_m(t/w)$ in order to determine $\lambda_s(t/w)$ is not enough since the simulations showed that the support will dent under a sample undergoing axial striction. The simulation also showed that a 10 μm layer of glue between sample and support changed $\lambda_s(t/w)$ by less than 2% for practical values of Young's modulus, hence this effect will be disregarded from now on. Calculations were done with a relative strain $\lambda_f = 1\%$, in the free sample.

3. Clamping

3.1. Mechanical clamping

An analytical calculation showed that a thin sample ($t/w \rightarrow 0$) on a rigid support has an axial striction $\lambda_s(0)$ which is expressed as a function of λ_f and ν_s by the equation

$$\lambda_s(0) = (1 - 2\nu_s)(1 - \nu_s)^{-1}\lambda_f, \quad t/w \rightarrow 0, \quad (1)$$

where ν_s is the Poisson's ratio of the sample.

This result makes three assumptions: that the support has no influence on the mechanism causing the original free striction λ_f ; that the sample must be isotropic; and that the volume of the sample remains constant. The heavy dots in fig. 2 are the result of eq. (1) and they agree very well with the results for η found through simulation. In order to show the linear relationship between η and t/w for $t/w \leq 0.1$ the horizontal axis of fig. 2 is linear for $t/w \leq 0.1$ and logarithmic for $t/w \geq 0.1$. It was found that $\lambda_s(0)$ was independent of E_0 if the ratio E_s/E_0 is smaller than 2.5, where E_s and E_0 are the Young's moduli of sample and support respectively. In this region of E_s/E_0 the support

may be described as rigid and eq. (1) will give the correct solution for $\lambda_s(0)$.

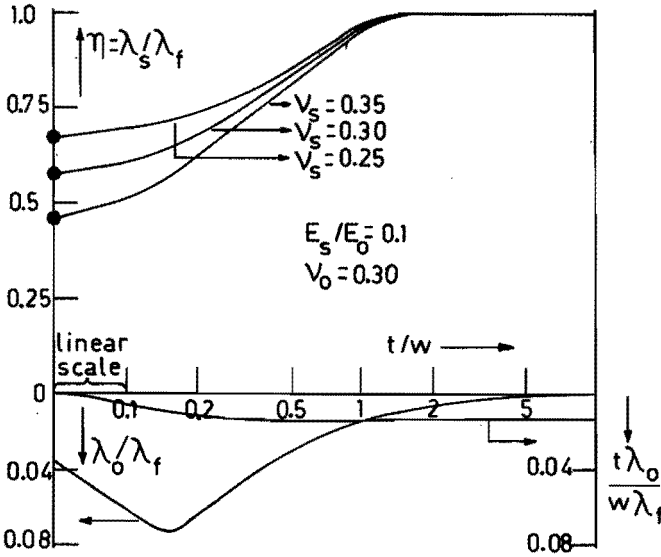


Fig. 2. The normalized clamped striction of a sample is shown as a function of t/w together with the normalized denting λ_o/λ_f of the support. The function $(\lambda_o/\lambda_f)(t/w)$ shows that the denting is constant when measured absolutely if $t/w > 0.3$.

3.2. Magnetostrictive or piezoelectric clamping

In eq. (1) the assumption has been made that the support has no influence on the mechanism causing the free striction. This is not true for anisotropic crystals which show magnetostriction or piezoelectricity. The striction in these crystals caused by magnetic or electric fields, respectively, is only possible in combination with transverse movements of the atoms in these crystals. Since these movements are prevented by the stresses exerted by the support on the sample, the free striction will be reduced to a value less than $\lambda_s(t/w)$.

4. Denting of the support

In calculating the denting of the support under the sample it is assumed that no external forces are exerted on the sample. The normalized dilatation $\lambda_0(t/w)/\lambda_f$ of the support is shown as a function of t/w in fig. 2. There is a linear relation between $\lambda_0(t/w)$ and t/w for $t/w \leq 0.1$. This relation is only slightly changed by varying ν_s .

δ is nearly linear function of E_s/E_0 as shown in fig. 3. The slope of the function depends on the value of ν_s/ν_0 , where ν_s and ν_0 are the Poissons ratios of the sample and support respectively. This is verified by setting ν_s and ν_0 at three different values while keeping ν_s/ν_0 constant. The simulations showed no difference in the results for δ . The denting of the support measured in absolute values is constant for $t/w \geq 0.3$ as shown by the function $t\lambda_0(t/w)/(w\lambda_f)$ in fig. 2.

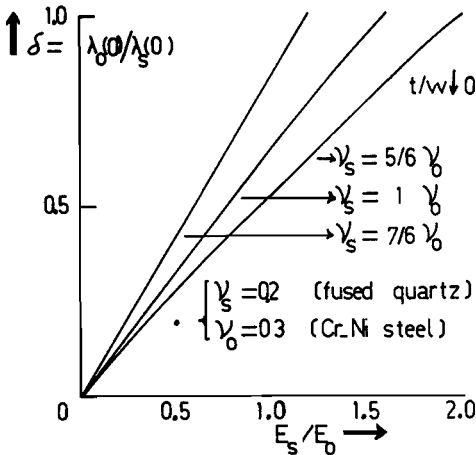


Fig. 3. The denting of the support $\lambda_0(0)$ normalized by the striction of the sample $\lambda_s(0)$ is shown as a function of the ratio of Young's moduli E_s/E_0 .

5. Measurement of the striction on quartz crystals

We used quartz crystals in our experiments because of their well known piezoelectric effect. A disadvantage is their anisotropy which required a detailed calculation (analytic) of the piezostriktion of a quartz crystal on a rigid support. By assuming that the support did not affect the piezoelectric mechanism in the crystal and using the values of the elastic constants quoted by Nye [4], it was calculated that the mechanically clamped sample would have a piezostriktion $\lambda_s(0)$ of 83% of the free striction (see appendix). However, an axial piezostriktion in quartz is accompanied by an equally large transverse striction of the free sample in one direction perpendicular to the axis. In samples with $t/w \leq 0.1$, half the striction, the transverse striction, is impossible. We assume that this limitation of the striction reduces the piezoelectric effect by $\frac{1}{2}$.

The denting of the support can be roughly estimated by using the E_s and ν_s of fused quartz.

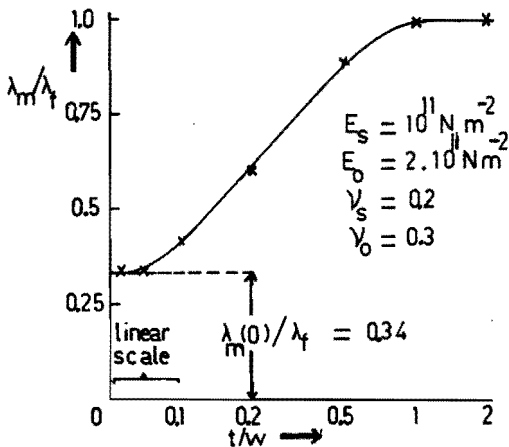


Fig. 4. Measurement of the striction λ_m of a quartz crystal along the piezoelectric axis. λ_m is normalized by the free striction λ_f of the quartz crystal.

These are given by Anderson [5] as 10^{11} N m^{-2} and 0.2, respectively. The support used in this experiment was made of Cr-Ni steel with an E_0 and ν_0 of $2 \times 10^{11} \text{ N m}^{-2}$ and 0.3, respectively. According to fig. 3 $\delta = 0.19$.

The measured dilatation of quartz should be

$$\lambda_m(0) = \lambda_s(0)(1 - \delta) \cdot \frac{1}{2}, \quad t/w \rightarrow 0. \quad (2)$$

Eq. (2) gives a value of $0.34\lambda_f$ for $\lambda_m(0)$. The experimental value found for $\lambda_m(0.02)$ was $0.34\lambda_f$, so this is in very good agreement with the value calculated above.

The experimentally measured curve of $\lambda_m(t/w)/\lambda_f$ for a quartz crystal is shown in fig. 4. In this experiment λ_f was about 10^{-6} .

6. Conclusions

The various strictions mentioned above are independent of a $10 \mu\text{m}$ layer of glue. The support can be assumed rigid in the calculation of the mechanical clamped striction, according to eq. (1), if $E_s/E_0 < 2.5$. The piezoelectric effect of quartz is limited by the support and this had to be taken into account in order to explain the experimentally measured striction of a thin quartz sample. This resulted in a factor of 0.5 in eq. (2).

The denting of the support is constant for samples with t/w greater than 0.3. In general, eq. (2) can be rewritten as

$$\lambda_m(0) = \lambda_s(0)(1 - \delta)c; \quad 0 < c < 1, \quad t/w \rightarrow 0,$$

where c is a constant which depends on the part of the mechanism of the striction in the sample which has been made impossible by the support.

Calculation of the mechanically clamped striction of a piezoelectric quartz crystal

A mechanically free quartz crystal with an electric field E applied to it shows the following strictions λ_i :

$$\lambda_1 = \lambda_1 = d_{11}E_1 \quad (\text{A. 1a})$$

$$\lambda_2 = -d_{11}E_1 \quad (\text{A. 1b})$$

$$\lambda_3 = \lambda_5 = \lambda_6 = 0 \quad (\text{A. 1c})$$

$$\lambda_4 = d_{14}E_1. \quad (\text{A. 1d})$$

The directions corresponding to the indices are shown in fig. 1a. The matrix for the piezoelectric constants d_{ij} of quartz crystals is given by Nye [4] (p. 126). The numbering of the indices is according to Voigt's notation.

When a thin quartz crystal ($t/w \rightarrow 0$) is attached to a rigid support λ_2 and λ_4 will be zero. This is caused by the stresses σ_2 , σ_3 and σ_4 exerted on the crystal by the support, the other stresses being zero. We use the values of the elastic constants S_{ij} of quartz given by Nye [4] to adapt eq. (A. 1) to the mechanically clamped condition. This leads to eq. (A. 2) for the mechanically clamped striction $\lambda_s(0)$ of quartz:

$$\lambda'_1 = \lambda_s(0) = S_{12}\sigma_2 + S_{13}\sigma_3 + S_{14}\sigma_4 + d_{11}E_1 \quad (\text{A. 1a})$$

$$\lambda'_5 = 0 = S_{11}\sigma_2 + S_{13}\sigma_3 - S_{14}\sigma_4 - d_{11}E_1 \quad (\text{A. 2b})$$

$$\lambda'_3 = 0 = S_{13}\sigma_2 + S_{33}\sigma_3 = \lambda'_5 = \lambda'_6 \quad (\text{A. 2c})$$

$$\lambda'_4 = 0 = -S_{14}\sigma_2 + S_{44}\sigma_4 + d_{14}E_1 \quad (\text{A. 2d})$$

where S_{11} , S_{12} , S_{13} , S_{14} , S_{33} and S_{44} are 1.27, -0.17, -0.15, -0.43, 0.97 and $2.01 \cdot 10^{-11} \text{ m}^2 \text{ N}^{-1}$, respectively, and d_{11} and d_{14} are 2.3×10^{-12}

and $0.67 \times 10^{-12} \text{ m V}^{-1}$, respectively. Simple calculation shows that $\lambda_s(0) = 0.83d_{11}E_1 = 0.83\lambda_f$.

References

- [1] P. van der Straten, Th. Kwaaitaal, W.M.M.M. van den Eijnden, J. Phys. Chem. Solids 41 (1980) 925.
- [2] Th. Kwaaitaal, J. Magn. Magn. Mat. 6 (1977) 290.
- [3] Aska Part 1 - Linear Static Analysis, QUAX 8, ISD Report no. 73, Stuttgart (1971).
- [4] J.F. Nye, Physical Properties of Crystals (Clarendon Press, Oxford, 1967) p. 148.
- [5] O.L. Anderson, in: Physical Acoustics, vol. III B, ed. W.P. Mason (Academic Press, New York, 1965) p. 87.

0304-8853/82/0000-0000/\$02.75 © 1982 North-Holland

7:2 Piezoelectric effect caused by second-harmonic distortion

In the electrostriction experiments we connected a high voltage amplifier to the sample. This amplifier has a second-harmonic distortion δV_{2f_0} superimposed on the signal V_{f_0} applied to the sample.

The signal δV_{2f_0} will cause dilatations $\delta(\Delta L_1)_{2f_0}$ in a piezoelectric sample. These piezoelectric dilatations have exact the same frequency as the electrostrictive ones. Hence they have to be kept as small as possible.

In figure 7.1 the dilatation $\delta(\Delta L_1)_{2f_0}$ of a quartz crystal is given versus δV_{2f_0} .

Reversing the electric field in the sample results in a sign reversal of $\delta(\Delta L_1)_{2f_0}$ as is expected from a piezoelectric dilatation. Figure 7.1 demonstrates that we are indeed measuring a piezoelectric effect. Even the absolute value of the piezoelectric constant $2.5 \times 10^{-12} \text{ m/V}$ calculated from this figure is in good agreement with the well known

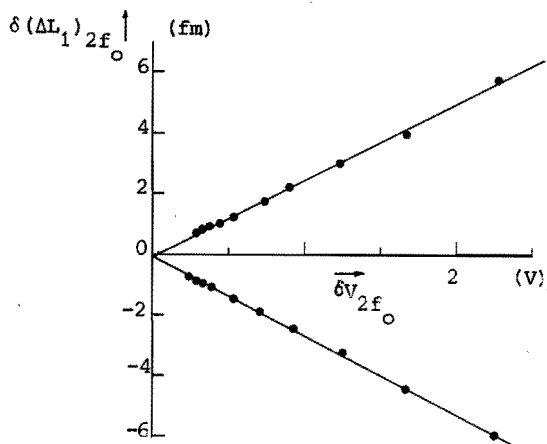


Figure 7.1 The piezoelectric dilatation $\delta(\Delta L_1)_{2f_0}$ caused by the second-harmonic distortion in the applied electric field. The electric field has been applied in two opposite directions.

value of $-2.3 \times 10^{-12} \text{ m/V}$ for quartz⁹.

By changing the d.c. offset of the signal V_{f_0} (300 V r.m.s.) it was possible to minimize δv_{2f_0} to less than 6 mV r.m.s. This corresponds to a second-harmonic distortion which was less than 2×10^{-5} . The dilatation $|\delta(\Delta L_1)_{2f_0}|$ will be lower than $0.006 \times 2.3 \times 10^{-12} \text{ m} = 15 \text{ fm}$. This is above the sensitivity of the interferometer which is 5 fm. Therefore we introduced a double sample. This is shown in figure 7.2.

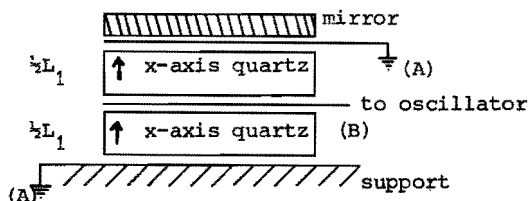


Figure 7.2 Orientation of the quartz crystals in a double sample.

The orientation of the x-axes of both quartz crystals is identical. The outside electrodes of the double sample are grounded. The middle electrode is connected to the high voltage amplifier. The piezoelectric dilatations of both quartz crystals are thus opposite in sign. Now we measure the overall linear piezoelectric effect of the double sample. This is less than 10% of the piezoelectric effect of a single quartz crystal. So $\delta(\Delta L_1)_{2f_0}$ is also reduced by a factor 10. The electrostrictive dilatations of each quartz crystal add. So the ratio between electrostrictive dilatations and $\delta(\Delta L_1)_{2f_0}$ increases 20 fold by using the double sample. After measuring the amplitude of a dilatation with frequency $2f_0$ we interchange the connections (A) and (B) on the double sample (see figure 7.2). Again we measure the amplitude of a dilatation with frequency $2f_0$. We now add both measurements and take half the sum. This gives us the electrostrictive dilatation $(\Delta L_1)_{2f_0}$ since the piezoelectric effect $\delta(\Delta L_1)_{2f_0}$ has been compensated by this method.

7:3 Measurement of electrostriction in quartz

We used two samples of Brasil x-cut quartz with a thickness L_1 of 2.96 mm. The samples are bought from the Dr. Neher Lab. in Leidschendam. We applied a signal with an amplitude of 424 V to the middle electrode of the double sample shown in figure 7.2. In another experiment we grounded the middle electrode and applied the same signal to the outer electrodes to correct for the second-harmonic distortion in the applied field. The electrostrictive dilatation $(\Delta L_1)_{2f_0}$ was the average of the measurements performed under the two described experimental conditions.

$(\Delta L_1)_{2f_0}$ was measured as a function of the frequency f_0 with

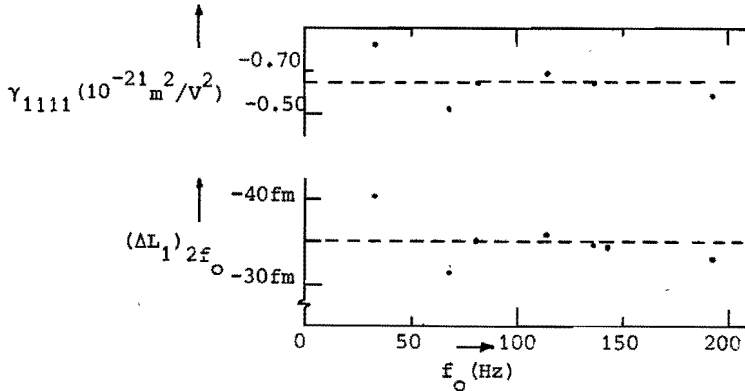


Figure 7.3 $(\Delta L_1)_{2f_0}$ and γ_{1111} determined as a function of the frequency f_0 on a double sample of quartz.

30 Hz < f_0 < 200 Hz. As expected $(\Delta L_1)_{2f_0}$ was independent of f_0 . The uncertainty in $(\Delta L_1)_{2f_0}$ is 7 fm.

$(\Delta L_1)_{2f_0}$ versus f_0 is shown in figure 7.3. The electrostrictive constant was calculated according to (3a) in section 2.1.

γ_{1111} versus f_0 is shown in figure 7.3. Using the error in $(\Delta L_1)_{2f_0}$ we calculated γ_{1111} of quartz:

$$\gamma_{1111} = (-6 \pm 2) \times 10^{-22} \text{ m}^2/\text{V}^2$$

We conclude that γ_{1111} is no function of the frequency in this frequency range.

We will now compare this result with the estimates given in chapter 3.

The discrepancy between our results and the experimental results of Gagnepain et al.³² has been discussed in section 2.1. It must be interpreted as second-harmonic distortion in their experiment. In our experiments this distortion is less than 1.5 fm or less than 5%

of $(\Delta L_1)_{2F_0}$. It does not play a role in view of the inaccuracy of about 30% in γ_{1111} .

The rough estimate based on dipole-dipole forces gives the correct absolute value of γ_{1111} . The estimate based on the pressure dependence of the refractive index gives the correct sign of γ_{1111} .

Table 7.1 Several estimated and experimental values of γ_{1111} in quartz.

	$\gamma_{1111} (10^{-21} \text{ m}^2/\text{V}^2)$
absolute value calculated from dipole-dipole forces (section 3.1)	0.66
minimum value calculated from the pressure dependence of the refractive index (section 3.2)	more negative than -0.15
γ_{1111} measured by Gagnepain ³²	25
our experimental value	-0.6 ± 0.2

8 Electrostriction in triglycine sulphate (TGS)

8:1 Data on TGS

TGS is a ferroelectric compound. It is soluble in water. Its solubility, as a function of temperature, is given by Nitsche³³. Single crystals of TGS are easily grown from a aqueous solution of 3 mol parts of glycine mixed with 1 mol part of H_2SO_4 . Glycine is also known as aminoacetic acid. It has the chemical formula NH_2CH_2COOH . The crystals are easily formed by letting the water slowly evaporate at room temperature. We have grown our own TGS single crystals with approximate dimensions of $10 \times 10 \times 6 \text{ mm}^3$. Some crystals were given to the Lab. for Organic Chemistry at our university. This laboratory verified the expected ratio of 3:17:6 between the numbers of N-, H- and C-atoms in TGS. The chemical formula of TGS is given by $(NH_2CH_2COOH)_3 \cdot H_2SO_4$.

TGS has been discovered to be a ferroelectric compound in 1956³⁴. Ferroelectric means that the substance has a spontaneous polarisation below the Curie temperature. This temperature³⁵ is $49.4^\circ C$. The spontaneous polarisation disappears gradually with increasing temperature and is zero at $49.4^\circ C$. This gradual disappearance is characteristic for a so called second-order transition.

The direction of the spontaneous polarisation lies parallel to the b-axis of a single domain crystal.

The dielectric constnt P'_0 along this axis is high and strongly temperature dependent. The electrostriction constant γ shows a quadratic dependence on P'_0 (see eq. (3.10)). Therefore it is interesting to measure γ as a function of temperature with the electric field along

the ferroelectric b-axis. The results of these measurements are shown in section 8.2.

TGS is piezoelectric below 49.4°C . So again we had to circumvent the influence of the second-harmonic distortion in the electric field, just as in quartz (see section 7.2). We did this by using a double sample. The samples are made in the following way.

TGS single crystals are easily cleaved along the plane perpendicular to the ferroelectric axis. This plane is used for orientation. The electric field lies in the direction of the ferroelectric axis. A sample is made by cleaving a single crystal twice at a distance of about 1 mm and sawing the resulting "plate" in two equal parts of $5 \times 6 \text{ mm}^2$. These parts are coated with silverpaint. They are set upon each other to form a double sample. More details on the preparation of this sample are given in section 4.2.

8:2 Theory and measurements

We present here the electrostriction constant γ of TGS, measured along the ferroelectric b-axis. We measured γ as a function of temperature. This function is quantitatively described by an extended theory of the second-order ferroelectric phase transition. The theoretical treatment is given in the following article³⁶ together with the experimental results.

ELECTROSTRICTION IN A UNIAXIAL FERROELECTRIC WITH SECOND ORDER PHASE TRANSITION

B.J. LUYMES

Department of Electrical Engineering, Eindhoven University of Technology, Eindhoven, The Netherlands

Received 18 February 1982

The electrostriction constant γ ($m^2 V^{-2}$) of a uniaxial ferroelectric with a second order phase transition has been calculated as a function of the dielectric constant $(\partial P/\partial E)_0$. The results have been experimentally verified on triglycine sulphate (TGS) by measuring γ and $(\partial P/\partial E)_0$. A sign reversal of γ above the Curie temperature is presented.

Predicting electrostrictive constants is difficult. For instance we used a first order Raylor expansion of the polarisation with respect to the electric field and predicted a positive electrostrictive constant in TGS. However we measured a negative one. We therefore introduce a second order approximation below, which explains this discrepancy well.

Electrostriction in uniaxial ferroelectrics is described by the following equation [1]

$$\Delta L/L = QP^2, \quad (1)$$

where $\Delta L/L$ is the relative change in thickness L of a sample in the direction of the polarisation P ($C\ m^{-2}$) along the ferroelectric axis. Q is a constant.

In electrostriction experiments, an electric field E is applied to a dielectric sample. The field E consists of an ac field ΔE superimposed on a much larger poling field E_0 . The minimum electric field strength has to be several times higher than the coercive field E_c in order to avoid hysteresis effects.

In general, electrostriction is described by

$$\Delta L/L = (\Delta L/L)_0 + (d_0 + \gamma\Delta E + \dots) \Delta E, \quad (2)$$

where d_0 (mV^{-1}) describes the linear converse piezoelectric effect. The electrostrictive coefficient is γ .

The index 0 refers to the situation in which $E = E_0$.

The coefficient γ can be expressed as a function of Q by expanding P in the second order Taylor expansion

$$P = P_0 + P'_0\Delta E + \frac{1}{2}P''_0\Delta E^2 + \dots, \quad (3)$$

where P_0 is the polarisation at $E = E_0$ and P'_0 and P''_0 are first and second order partial derivatives of P with respect to E . Combining eqs. (1), (2) and (3) leads to

$$\gamma = Q(P_0'^2 + P_0P_0''), \quad d_0 = 2QP_0P_0',$$

$$(\Delta L/L)_0 = QP_0^2. \quad (4)$$

Our experiments on a uniaxial ferroelectric crystal TGS resulted in a negative value for γ/Q below the transition (Curie) temperature T_c ($49.4^\circ C$, [3]). According to eq. (4) such a negative value of γ/Q can be explained by a negative value of P_0'' .

The sign of P_0'' can be deduced from the expression of the elastic Gibbs energy G ($J\ m^{-3}$) for a uniaxial ferroelectric crystal [4]

$$G = G_1 - EP + \frac{1}{2}\beta(T - T_c)P^2 + \frac{1}{4}\delta P^4, \quad (5)$$

where $|G_1|$, β and δ are positive constants. T stands for temperature. Differentiating G with respect to P and then twice more with respect to E leads to

$$P_0'' = -6\delta P_0 P_0'^3. \quad (6)$$

Thermal equilibrium has been assumed, so that $\partial G/\partial P = 0$. The positive signs of P_0 and P_0' result in an expected negative value of P_0'' in eq. (6). Combining eqs. (4) and (6) leads to

$$\gamma = QP_0'^2(1 - 6b), \quad b = \delta P_0^2 P_0', \quad 0 < b < \frac{1}{2}. \quad (7)$$

The coefficient γ will now be analysed as a function of T . At temperatures below T_c the factors P_0^2 and P_0' are equal to $\beta(T_c - T)/\delta$ and $\frac{1}{2}\beta^{-1}(T_c - T)^{-1}$, respectively [4]. This leads to $b \uparrow \frac{1}{2}$. Above T_c the factors P_0 and P_0' are roughly proportional to $(T - T_c)^{-1}$ [4], leading to $b \downarrow 0$. The result is $0 < b < \frac{1}{2}$, as shown in eq. (7).

Calculating $\partial^2 G/\partial P \partial E$ and $\partial G/\partial P$ from eq. (5) and replacing $\delta P_0^2 P_0'$ by b gives

$$T = T_c + [(1 - 3b)/\beta] [\delta E_0^2/b(1 - 2b)^2]^{1/3}. \quad (8)$$

A relation between γ and P_0' can be derived from calculating $\partial^2 G/\partial T \partial P$ and $\partial^2 G/\partial E \partial P$. This leads first to

$$\partial P_0/\partial T = -\beta P_0 P_0'. \quad (9)$$

Differentiating eq. (9) with respect to E and supplementing with eq. (4) gives

$$\gamma = -(Q/\beta) \partial P_0'/\partial T. \quad (10)$$

All calculations are done under isothermal conditions. Differentiating eq. (7) with respect to T and eliminating $\partial P_0/\partial T$ and $\partial P_0'/\partial T$ according to eqs. (9) and (10), respectively, leads to eq. (11), if γ is eliminated finally as given in eq. (7)

$$\partial\gamma/\partial T = -2QP'_0{}^3\beta(1-3b)(1-18b). \quad (11)$$

According to eq. (7), γ shows a sign reversal if $b = 1/6$. The temperature T_1 at which this happens can be calculated from eq. (8). According to eq. (11) γ has extrema at temperatures T_c and T_2 if $b = 1/3$ and $b = 1/18$, respectively. T_c and T_2 can also be calculated with the aid of eq. (8). The extrema of γ , i.e. $\gamma(T_c)$ and $\gamma(T_2)$, are calculated by analogy with the calculations leading to eq. (8):

$$\gamma(T_c) = -\frac{1}{9}Q(\delta E_0^2)^{-2/3}, \quad (12)$$

$$\gamma(T_2) = \left(\frac{2}{3}\right)^5 Q(2\delta E_0^2)^{-2/3}. \quad (13)$$

The above described theory of γ as a function of temperature has been verified on TGS. Fig. 1 shows both γ and $\partial P'_0/\partial T$. The electrostrictive dilatation $\gamma\Delta E^2$ has been measured by a lock-in technique in an electronically stabilized Michelson interferometer [5].

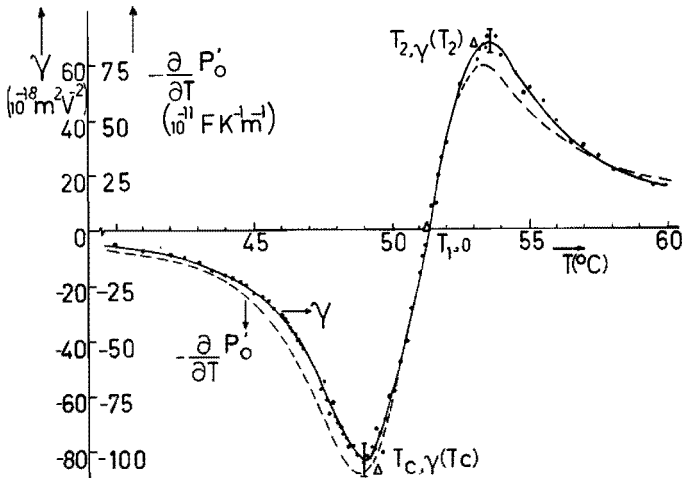


Fig. Both the electrostriction constant γ and the temperature derivative of the dielectric constant P'_0 of the electrical poled TGS are shown as a function of temperature. An ac measurement determines P'_0 . The broken line shows $\partial P'_0/\partial T$. The triangles show calculated points of γ according to eqs. (8), (12) and (13).

P'_0 has been measured by a Sawyer–Tower circuit [6]. An arbitrary frequency of 67 Hz was used in both cases.

Earlier experiments on TGS [7] showing a dependence of γ on E_0 , do not show a sign reversal of γ as a function of temperature, since these experiments have been performed without a poling field. In our experiments $E_0 = 500$ V/mm and $\Delta E = 80$ V/mm. Hysteresis effects are avoided since $E_c(\text{TGS}) \leq 40$ V/mm above 20°C [8].

$\gamma(T_c)$, T_1 and $\gamma(T_2)$ are calculated for TGS. The results are marked by triangles in fig. 1. We used $Q = +2.35 \text{ C}^{-2}\text{m}^4$ [9], $\beta = +3.5 \times 10^7 \text{ F}^{-1}\text{K}^{-1}\text{m}$ [10] and $\delta = +6.5 \times 10^{11} \text{ F}^{-1}\text{C}^{-2}\text{m}^5$ [10]. The value of Q for TGS is constant [11].

Calculating $\gamma^{-1} \partial P'_0 / \partial T$ for each temperature interval of 1 K from 22°C to 60°C leads to a value of β/Q of $(1.5 \pm 0.25) \times 10^7 \text{ J m}^{-3}\text{K}^{-1}$ according to eq. (10). The results of β/Q are shown in fig. 2 and are in good agreement with the figures for β and Q mentioned above.

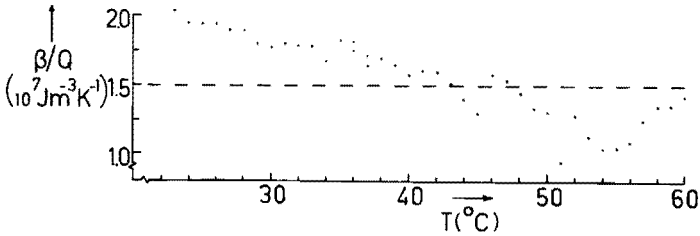


Fig. 2. The coefficient $\beta/Q = -(\partial P'_0 / \partial T) / \gamma$ has been calculated for TGS for different temperatures. The broken line gives the expected value of β/Q according to refs. [9,10].

An inaccuracy in the temperature measurement of 0.5 K caused by a temperature gradient between thermocouple and TGS crystal led to scattering when measuring T_c , T_1 and T_2 . The agreement between the

calculated and measured values of the extrema of γ is good, as shown in fig. 1.

Strictly speaking an adiabatic correction $[1 + b\beta^2/\delta C_p(T_c - T)]$ in the right-hand side of eq. (10) should be introduced. This first order approximation has been calculated, since γ , Q and P'_0 are experimentally determined adiabatically. C_p is the heat capacity at constant polarisation and is minimal $2.6 \times 10^6 \text{ J m}^{-3}\text{K}^{-1}$ for TGS [8]. In calculating the adiabatic correction we used the method given by Devonshire [1]. The correction is less than 1% in TGS and may be neglected in view of the experimental uncertainties in γ , Q and P'_0 .

References

- [1] A.F. Devonshire, *Adv. Phys.* 3 (1954) 99.
- [2] J.F. Nye, *Physical properties of crystals* (Clarendon, Oxford, 1969).
- [3] T. Mitsui, *An introduction to the physics of ferroelectrics* (Gordon and Breach, New York, 1976).
- [4] E. Fatuzzo and W.J. Merz, *Selected topics in solid state physics*, Vol. VII (North-Holland, Amsterdam, 1967).
- [5] Th. Kwaaitaal, B.J. Luymes and G.A. van der Pyll, *J. Phys. D13* (1980) 1005.
- [6] C.B. Sawyer and C.H. Tower, *Phys. Rev.* 35 (1930) 269.
- [7] A.A. Fotchenkov and M.P. Zaitseva, *Sov. Phys. Crystallogr.* 8 (1964) 579.
- [8] Landolt-Bornstein, Vol. III, no. 3 (Springer, Berlin, 1969) pp. 495, 496.
- [9] G. Schmidt and P. Pfannschmidt, *Phys. Stat. Sol.* 3 (1963) 2215.
- [10] S. Triebwasser, *IBM J. Res.* July (1958) 212.
- [11] K.H. Ehses and H. Meister, *Ferroelectrics* 25 (1980) 573.

8:3 Details on the adiabatic correction

In section 8.2 we derived the equation

$$\gamma = \frac{-Q}{\beta} \frac{\partial P'_O}{\partial T} \quad (8.1)$$

In this relation we deal with γ_T and Q_T where the index T refers to the isothermal condition. Now we will express (8.1) in γ_S and Q_S since our measurements were done under adiabatic conditions, denoted by the index S. The numerical correction will prove to be very small.

The following expressions are used for γ_T and Q_T

$$\begin{aligned} \gamma_T &\equiv \left(\frac{\partial \Delta L/L}{\partial E^2} \right)_T = \frac{1}{2E} \left(\frac{\partial \Delta L/L}{\partial E} \right)_T = \frac{(P'_O)_T}{2E} \left(\frac{\partial \Delta L/L}{\partial P} \right)_T = \\ &= (1 + k_1 T) k_2 \frac{(P'_O)_S}{2E} \left(\frac{\partial \Delta L/L}{\partial P} \right)_S \equiv (1 + k_1 T) k_2 \gamma_S \\ Q_T &\equiv \left(\frac{\partial \Delta L/L}{\partial P^2} \right)_T = \frac{1}{2P} \left(\frac{\partial \Delta L/L}{\partial P} \right)_T = \frac{k_2}{2P} \left(\frac{\partial \Delta L/L}{\partial P} \right)_S \equiv k_2 Q_S \end{aligned}$$

with $\frac{\Delta L}{L} = \gamma E^2 = Q P^2$, the electric field E larger than the coercive field E_c ,

$$(P'_O)_T \equiv (P'_O)_S (1 + k_1 T)$$

and

$$\left(\frac{\partial \Delta L/L}{\partial P} \right)_T \equiv k_2 \left(\frac{\partial \Delta L/L}{\partial P} \right)_S \quad (8.2)$$

This last assumption will be checked later on.

Using the expressions for γ_T , Q_T and $(P'_O)_T$ in (8.1) gives

$$\gamma_S = \frac{-Q_S}{\beta} \frac{\partial (P'_O)_S}{\partial T} \left[1 + \frac{k_1}{1 + k_1 T} \frac{\partial T}{\partial \ln P'_O} \right] \quad (8.3)$$

We leave out the index S of P'_O between the square brackets, since we are dealing with a correction factor. This factor is estimated in the following way. According to Devonshire⁸

$$\frac{1}{(P'_O)_S} = \frac{1}{(P'_O)_T} + T \left(\frac{\partial E}{\partial T} \right)_P^2 / C_P \quad (8.4)$$

The factor $\left(\frac{\partial E}{\partial T} \right)_P$ is easily calculated from equation 5 in section 8.2. It equals βP . We derive an expression for k_1 in a straightforward way from (8.2), so

$$k_1 = \beta^2 P^2 P'_O / C_P = b\beta^2 / (C_P \delta), \text{ with } k_1 T \ll 1 \quad (8.5)$$

The numerical values of the constants are given in section 8.2 for TGS. We see that the assumption made in (8.2) agrees with (8.4). The assumption $k_1 T \ll 1$ is correct for TGS as $k_1 = 3.6 \times 10^{-4} (\text{K}^{-1})$ and $T \leq 333 \text{ K}$ in our experiments. From equation 5 in section 8.2 it is easily seen that

$$\frac{\partial T}{\partial \ln P'_O} = T_C - T \quad (8.6)$$

Using (8.5) and (8.6) in (8.3) leads to

$$\gamma_S = \frac{-Q_S}{\beta} \frac{\partial (P'_O)_S}{\partial T} \left[1 + \frac{b\beta^2 (T_C - T)}{C_P \delta} \right]$$

So the adiabatic correction of (8.1) amounts to $k_1 (T_C - T) \times 100\%$ or about 1% for TGS. It may be neglected in view of the experimental errors.

9 Summary and conclusions

Electrostriction occurs in every material. It causes very small dilatations in our experiments. They are of the order of 10^{-13} m. The ferroelectric compounds are an exception since the electrostrictive dilatations in these compounds are several orders of magnitude larger. The very small dilatations accompanying the phenomenon of electrostriction are detected in a stabilized Michelson interferometer. The sensitivity of this specially designed interferometer is such that it is easy to detect vibrations with an amplitude down to 5×10^{-15} m. This amplitude is of the same order as the fundamental limit set by the photon character of the light impinging on the photodiode of the interferometer.

Electrostriction is described by the electrostriction coefficient γ (m^2/V^2). This coefficient describes the quadratic relationship between the strain $\Delta L/L$ and applied electric field E

$$\Delta L/L = \gamma E^2$$

A compound may either contract ($\gamma < 0$) or expand ($\gamma > 0$) in an applied electric field. In order to determine the sign of γ we compare the images of two signals on an oscilloscope. One signal originated from a contracted piezoelectric quartz crystal and the other from the electrostrictive dilatation of the compound to be studied. (chapter 2)

In order to estimate the electrostrictive strains that can be expected, we studied a simple model for electrostriction. This mechanism is based on the forces between dipoles induced by the electric field. The model proposed results in

$$|\gamma| = \frac{6}{4\pi} S_{11} \epsilon_0 (\epsilon_r - 1)^2$$

where ϵ_0 (F/m) is the dielectric constant of vacuum, S_{11} (m^2/N) a component of the elastic compliance tensor and ϵ_r the relative dielectric constant. This model gives the correct order of magnitude of γ as observed in a number of crystals. The model does not take into account the actual crystal structure. In the case of diamond, where we did take into account its crystal structure, we also found the correct sign of γ (section 6.2). In general the sign of γ is opposite to that of the derivative of the refraction index n with respect to the hydrostatic pressure. The absolute value of this derivative gives an estimate of the minimum value of $|\gamma|/(n\epsilon_0)$. (chapter 3)

We use an a.c. method to detect electrostrictive dilatations. Great care has been taken to circumvent spurious signals resulting from mechanical resonance. This has been done by choosing the right measurement frequency. We measure the electrostriction of mechanically free samples. Further details on the sample preparation are given. (chapter 4)

Values of γ have been experimentally determined for LiF (chapter 5), diamond (chapter 6), quartz (chapter 7) and triglycine sulphate or TGS (chapter 8).

The way to cope with "large" piezoelectric effects is by stacking two identically orientated single crystals on top of each other. (chapter 7)

A detailed theory of γ as a function of temperature near the Curie temperature T_c is given for ferroelectric crystals with a second order transition at T_c . We describe and use a method which enables us to measure γ continuously as a function of temperature around T_c . There is quantitative agreement between theory and experiments on ferroelectric single crystals of triglycine sulphate. (chapter 8)

Notation index

indices and suffixes:			They stand for:
a			average
f			frequency, free moving or feedback
f_o			oscillator frequency
i, j, k, l			specific directions in a single crystal, they are 1, 2 or 3
m			measured quantity
n			noise
o			stationary condition or support
P			constant polarisation
q			quartz
S			adiabatic conditions
s			signal or sample
T			isothermal condition
Symbols	Units	description	
α	-	optical loss factor in the interferometer	
λ	m	Angstrom	
γ	$m^2 V^{-2}$	component of an electrostriction tensor	
C, c	-	constant between zero and one	
C_p	$Jm^{-3} K^{-1}$	heat capacity at constant polarisation	
d_{ijk}	mV^{-1}	component of a piezoelectric tensor	
D	Cm^{-2}	component of the dielectric displacement vector	

ϵ_0	Fm^{-1}	dielectric constant of vacuum: 8.8542×10^{-11}
ϵ_r	-	relative dielectric constant
E	Vm^{-1}	component of the electric field vector
E_c	Vm^{-1}	coercive field
E_o, E_s	Nm^{-2}	Young's moduli
F	N	component of the force vector
\vec{F}	N	force vector
f	Hz	frequency
Δf	Hz	width of a frequency band
f_o	Hz	oscillator frequency
G	Jm^{-3}	free Gibbs energy
g_{ijk}	$\text{m}^2 \text{C}^{-1}$	component of a piezoelectric tensor
η	-	efficiency defined in each relevant section
h	Ws^2	Planck's constant: 6.63×10^{-34}
I, i	A	total current and signal current, respectively
J	Wm^{-2}	luminous intensity on a photodiode
$\tilde{\Delta J}$	Wm^{-2}	amplitude of noise in J
$\tilde{\delta J}$	Wm^{-2}	amplitude of noise, apparently in J
λ	m	wavelength of laserlight
$\lambda_f, \lambda_m, \lambda_o, \lambda_s$	-	strains
L	m	length
$L_2 - L_1$	m	difference in length between the two interferometer arms
ΔL	m	relatively small change in length
$\Delta L'$	m	apparent displacement caused by refractive index noise
$\Delta L_i / L_j$	-	component of the strain tensor

$(\Delta L/L)_c$	-	apparent strains caused by Coulomb forces acting on the electrical connections to the sample
$\delta (\Delta L_1)_{2f_0}$	m	dilatations caused by second-harmonic distortion
$[(\Delta L_1)_{2f_0}]_{sp}$	m	spurious dilatations with frequency $2f_0$
ν	Hz	frequency of lightwaves
ν_o, ν_s	-	Poisson's ratios
N		noise
n_{ij}	-	component of the refractive index tensor
P	Cm^{-2} or W	component of the polarisation vector or the power of light impinging on a photodiode
\vec{P}	Cm^{-2}	polarisation vector
P'	Fm^{-1}	derivative of P with respect to E
P_o	Cm^{-2}	polarisation at field E_o
P_o'	Fm^{-1}	derivative of P_o with respect to E, at E_o
P_o''	C	second derivative of P_o with respect to E, at E_o
p	Cm	magnitude of a dipole moment
\vec{p}	Cm	dipole moment vector
Q_{ijkl}	$m^4 C^{-2}$	component of an electrostriction tensor
q	C	charge
R_f	Ω	feedback resistor
r	m	distance
σ	Nm^{-2}	hydrostatic pressure
σ_{ij}	Nm^{-2}	component of the stress tensor
S	Jk^{-1}	entropy
S_{ijkl}, S_{ij}	$m^2 N^{-1}$	component of the elastic compliance tensor
T	K	temperature
T_c	K	Curie temperature
t/w	-	thickness to width ratio

U	Jm^{-3}	internal energy
ϕ	Jm^{-3}	free energy
ϕ	-	phase
V_{tt}	V	represents the difference between maximum and minimum of the interference pattern
δV_{2f_0}	V	second-harmonic distortion
x	m	static displacement
x	m	dynamic displacement
Δx	m	small distance in the direction of the x-axis
(x,y,z)	-	refers to the three orthogonal axes

References:

- [1] Slack, G.A. and S.F. Bartram
THERMAL EXPANSION OF SOME DIAMONDLIKE CRYSTALS.
J. Appl. Phys., Vol. 46(1975), p. 89-98.
- [2] Zeyen, C.M.E. and H. Meister
ORDER PARAMETER OF THE KDP FERROELECTRIC PHASE TRANSITION
MEASURED BY THE NEUTRON DIFFRACTOMETRY.
3rd European Meeting on Ferroelectricity (EMF-3); Zürich,
22-26 Sept. 1975.
Ferroelectrics, Vol. 14(1976), p. 731-734.
- [3] Ehse, K. H. et al.
THE THERMAL EXPANSION OF TGS.
4th Int. Meeting on Ferroelectricity (IMF-4); Leningrad,
18-23 Sept. 1977.
Ferroelectrics, Vol. 20(1978), p. 287-288.
- [4] Bohatý, L. and S. Haussühl
QUADRATIC ELECTROSTRICTIVE EFFECTS IN LiF, NaF, NaCl,
NaBr, KCl, KBr, KI, RbCl, RbBr and RbI.
Acta Crystallogr. Sect. A, Vol. A33(1977), p. 114-118.
- [5] Vilkomerson, D.
MEASURING PULSED PICOMETER-DISPLACEMENT VIBRATIONS BY
OPTICAL INTERFEROMETRY.
Appl. Phys. Lett., Vol. 29(1976), p. 183-185.
- [6] Uchino, K. and L.E. Cross
A VERY HIGH SENSITIVITY AC DILATOMETER FOR THE DIRECT
MEASUREMENT OF PIEZOELECTRIC AND ELECTROSTRICTIVE CONSTANTS.
1979 IEEE Int. Symp. on Applications of Ferroelectrics;
Minneapolis, Minnesota, 13-15 June 1979.
Ferroelectrics, Vol. 27(1980), p. 35-39.
- [7] Kwaaitaal, Th., B.J. Luymes and G.A. van der Pijll
NOISE LIMITATIONS OF MICHELSON LASER INTERFEROMETERS.
J. Phys. D, Vol. 13(1980), p. 1005-1015. (Section 2.1 of this thesis).
- [8] Devonshire, A.F.
THEORY OF FERROELECTRICS.
Adv. Phys., Vol. 3(1954), p. 85-130.
- [9] Nye, J.F.
PHYSICAL PROPERTIES OF CRYSTALS: Their representation
by tensors and matrices.
Oxford University Press, 1957.
- [10] Shirane, G. and K. Sato
EFFECTS OF MECHANICAL PRESSURES ON THE DIELECTRIC PROPERTIES
OF POLYCRYSTALLINE BARIUM-STRONTIUM TITANATE.
J. Phys. Soc. Jpn., Vol. 6(1951), p. 20-26.

- [11] Mason, W.P.
THE ELASTIC, PIEZOELECTRIC, AND DIELECTRIC CONSTANTS OF POTASSIUM DIHYDROGEN PHOSPHATE AND AMMONIUM DIHYDROGEN PHOSPHATE.
Phys. Rev., Vol. 69(1946), p. 173-194.
- [12] Zheludev, I.S. and A.A. Fotchenkov
ELECTROSTRICTION OF LINEAR DIELECTRICS.
Sov. Phys. - Crystallogr., Vol. 3(1958), p. 312-318.
- [13] Schmidt, G. und P. Pfannschmidt
PIEZOELEKTRIZITÄT UND ELEKTROSTRIKTION DES TRIGLYZINSULFATS.
Phys. Status Solidi, Vol. 3(1963), p. 2215-2220.
- [14] Link, J. et al.
PRESSURE VARIATION OF THE LOW-FREQUENCY DIELECTRIC CONSTANTS OF SOME ANISOTROPIC CRYSTALS.
J. Appl. Phys., Vol. 52(1981), p. 936-939.
- [15] Waxler, R.M. and C.E. Weir
EFFECT OF HYDROSTATIC PRESSURE ON THE REFRACTIVE INDICES OF SOME SOLIDS.
J. Res. Natl. Bur. Stand. Sect. A, Vol. 69A(1965), p. 325-333.
- [16] Fotchenkov, A.A.
APPARATUS FOR MEASURING VERY SMALL DISPLACEMENTS OF OSCILLATING CRYSTALS.
Sov. Phys. - Crystallogr., Vol. 2(1957), p. 643-647.
- [17] CRC HANDBOOK OF CHEMISTRY AND PHYSICS. Ed. by R.C. Weast.
53rd ed.
Cleveland, Ohio: Chemical Rubber, 1972. P. E210.
- [18] Dandridge, A. and A.B. Tveten
PHASE NOISE OF SINGLE-MODE DIODE LASERS IN INTERFEROMETER SYSTEMS.
Appl. Phys. Lett., Vol. 39(1981), p. 530-532.
- [19] Landolt-Börnstein
NUMERICAL DATA AND FUNCTIONAL RELATIONSHIPS IN SCIENCE AND TECHNOLOGY. New series. Group III: Crystal and solid state physics. Vol. 17a: Semiconductors. Physics of group IV elements and III-V compounds. Ed. by O. Madelung.
Berlin: Springer, 1982. P. 36.
- [20] Spangenberg, K. und S. Haussühl
DIE ELASTISCHE KONSTANTEN DER ALKALIHALOGENIDEN VOM STEINSALZ-TYPUS.
Z. Kristallogr., Vol. 109(1957), p. 422-437.
- [21] Haussühl, S.
DAS DIELEKTRISCHE VERHALTEN DER ALKALIHALOGENIDEN VOM STEINSALZ-TYPUS.
Z. Naturforsch. a, Vol. 12a(1957), p. 445-447.

- [22] Landolt-Börnstein
 NUMERICAL DATA AND FUNCTIONAL RELATIONSHIPS IN SCIENCE
 AND TECHNOLOGY. New series. Group III: Crystal and solid
 state physics. Vol. 3: Ferro- and antiferroelectric
 substances. Ed. by K.-H. Hellwege and A.M. Hellwege.
 Berlin: Springer, 1969. P. 492.
- [23] Uchino, K. and L.E. Cross
 ELECTROSTRICTION AND ITS INTERRELATION WITH OTHER ANHARMONIC
 PROPERTIES OF MATERIALS.
 Jpn. J. Appl. Phys., Vol. 19(1980), p. L171-L173.
- [24] Kwaaitaal, Th.
 SUB-ANGSTROM MAGNETOSTRICTIVE DILATATIONS INVESTIGATED
 WITH AN OPTICAL INTERFEROMETER.
 Ph.D. Thesis. Eindhoven University of Technology, 1980.
- [25] Cullity, B.D.
 ELEMENTS OF X-RAY DIFFRACTION.
 Reading, Mass.: Addison-Wesley, 1956.
Addison-Wesley series in metallurgy and materials
- [26] Bohatý, L.
 QUADRATISCHE ELEKTROSTRIKTIVE EFFEKTE IN KRISTALLEN.
 Ph.D. Thesis. Universität zu Köln, 1975.
- [27] Haussühl, S. und G. Walda
 MESSUNG DES ABSOLUTEN QUADRATISCHEN ELEKTROOPTISCHEN
 EFFEKTS IN KRYSTALLEN: Beispiele LiF und α -TiAl(SO₄)₂.12H₂O.
 Phys. Status Solidi a, Vol. 5(1971), p. K163-K165.
- [28] Born, M. and E. Wolf
 PRINCIPLES OF OPTICS: Electromagnetic theory of propagation,
 interference and diffraction of light.
 London: Pergamon, 1959.
- [29] Luymes, B.J.
 INTERFEROMETRIC MEASUREMENTS OF VERY SMALL ELECTROSTRICTIVE
 STRAINS.
 To be published in January 1983 by the journal "Review of Scientific
 Instruments". The text is presented in section 2.1 of this thesis.
- [30] Maradudin, A.A. and E. Burstein
 RELATION BETWEEN PHOTOELASTICITY, ELECTROSTRICTION, AND
 FIRST-ORDER RAMAN EFFECT IN CRYSTALS OF THE DIAMOND STRUCTURE.
 Phys. Rev., Vol. 164(1967), p. 1081-1099.
- [31] Kwaaitaal, Th., B.J. Luymes and W.M.M.M. van den Eijnden
 CALCULATION AND MEASUREMENT OF MAGNETOSTRICTIVE CONSTANTS OF
 THIN LAYERS.
 J. Magn. & Magn. Mater., Vol. 26(1982), p. 187-190.
 Text is presented in section 7.1 of this thesis.

- [32] Gagnepain, J.J. and R. Besson
NONLINEAR EFFECTS IN PIEZOELECTRIC QUARTZ CRYSTALS.
In: PHYSICAL ACOUSTICS: Principles and methods. Vol. 11.
Ed. by W.P. Mason and R.N. Thurston.
New York: Academic Press, 1975. P. 245-288.
- [33] Nitsche, R.
GROWTH OF FERROELECTRIC CRYSTALS OF THE TYPE $(\text{Glycine})_3\text{H}_2\text{AB}_4$.
Helv. Phys. Acta, Vol. 31(1958), p. 306-308.
- [34] Matthias, B.T. et al.
FERROELECTRICITY OF GLYCINE SULFATE.
Phys. Rev., Vol. 104(1956), p. 849-850.
- [35] Mitsui, T. et al.
AN INTRODUCTION TO THE PHYSICS OF FERROELECTRICS.
New York: Gordon & Breach, 1976.
Ferroelectricity and related phenomena
- [36] Luymes, B.J.
ELECTROSTRICTION IN A UNIAXIAL FERROELECTRIC WITH SECOND-ORDER
PHASE TRANSITION.
Physics Letters A, Vol. 90A (1982), P. 313-315.
The text is presented in section 8.2 of this thesis.
- [37] Grindlay, J. and H.C. Wong
ON THE THEORY OF ELECTROSTRICTION IN FINITE IONIC CRYSTALS:
NON-PIEZOELECTRIC CASE.
Can. J. of Phys., Vol. 47 (1969), P. 1563-1571.

Toelichting bij de in dit proefschrift opgenomen artikelen.

Hieronder volgt een nadere aanduiding van de bijdragen van medeauteurs aan de in dit proefschrift opgenomen artikelen. Hiermee wordt voldaan aan art. 13 van het promotie-reglement.

1) Noise limitations of Michelson laser interferometers (hfdst. 2).

Dr. Ir. Th. Kwaaitaal heeft twee gedeelten uitgewerkt i) Het effect van shotnoise op de gevoeligheid van de elektronisch gestabiliseerde interferometer en het effect van andere ruisbronnen op de gevoeligheid van Michelson interferometers.

Ir. G.A. van der Pijll verrichtte in het kader van zijn afstudeerwerk de meeste metingen die in dit artikel gepresenteerd zijn.

2) Calculation and measurement of magnetostrictive constants of thin layers (hfdst. 7).

Dr. Ir. Th. Kwaaitaal heeft het experiment met de bijbehorende computer simulatie voorgesteld en heeft deze simulatie mede uitgevoerd.

Ing. W.M.M.M. van den Eijnden heeft de experimenten die in dit artikel gepresenteerd worden uitgevoerd.

DANKWOORD

De afgelopen vier jaren heb ik met veel plezier gewerkt in de vakgroep Elektrotechnische Materiaalkunde van de T.H. Eindhoven. Dit proefschrift is dan ook tot stand gekomen in prettige samenwerking met alle leden van deze groep. Op praktisch-technisch gebied was W.M.M.M. van den Eijnden onmisbaar bij het prepareren van samples en het onderhouden van de contacten met de afdelingswerkplaats van de afdeling der Elektrotechniek. Allen die aan deze werkplaats verbonden zijn wil ik graag bedanken voor het maken van de verschillende onderdelen van de interferometer.

Het verzorgen van de referenties door I.V. Brûzã betekende een flinke taakverlichting voor mij.

Mevr. J.H.M.G. Coppens en mevr. C.M. Bijl ben ik dankbaar voor het uittypen van het manuscript plus de tijdrovende toevoegingen.

CURRICULUM VITAE

- 21-1-1953 geboren te Huntly (Nieuw-Zeeland).
- 1971 HBS-B diploma behaald aan het 1^{ste} Chr. Lyceum te Haarlem.
- 1977-1978 Student assistent in de vakgroep Lage Temperaturen, afd. Technische Natuurkunde van de T.H. te Delft.
- 1978 Ingenieursdiploma behaald aan de T.H. Delft in de richting Technische Natuurkunde.
(afstudeeronderwerp: uitzettingscoëfficiënten bij lage temperaturen).
- 1978-1982 Wetenschappelijk assistent in de vakgroep Elektrotechnische Materiaalkunde, afd. Elektrotechniek van de T.H. te Eindhoven.

STELLINGEN

B.J. Luymes

17 december 1982

I. Bij de bestudering van de geleiding in ZnO varistors geeft men vaak de stroom-spannings-karakteristiek weer op dubbellogaritmische schaal ($\log I/I_0 - \log V/V_0$). Het is beter dit te doen op enkellogaritmische schaal ($\log I/I_0 - V$).

- 1] L.M. Levinson and H.R. Philipp, The physics of metal oxide varistors, J. Appl. Phys., Vol. 46, (1975), p. 1332-1341.
- 2] K. Eda, Conduction mechanism of non-ohmic zinc oxide ceramics, J. Appl. Phys., Vol. 49, (1978), p. 2964-2972.

II. Het verschil tussen de gemeten en geschatte elektrostrictie coëfficiënt van LiF is groot.* De oorzaak van dit verschil moet gezocht worden in het ionogeen-karakter van LiF.

* hfdst. 3 van dit proefschrift.

III. De grenzen van het meetbare zijn niet bereikt met de meetmethode die in dit proefschrift beschreven is. Optische vermenigvuldiging van de te meten verplaatsing geeft nieuwe mogelijkheden.

IV. In het artikel van J.L.M.J. van Bree et.al. is de detectielimiet van een lineaire verplaatsingsopnemer onvolledig gegeven, daar de frequentie-afhankelijkheid van de limiet, t.g.v. het skineffect in ferromagnetische kernen, niet meegenomen is.

J.L.M.J. van Bree, J.A. Poulis and F.N. Hooge,
Barkhausen noise in differential transfor-

mers, Appl.Sci.Res., Vol. 30, (1975),
p.304-308.

V. Het verschil in de gemiddelde lichtintensiteit van de twee, reeds geïnterfereerd hebbende, laserbundels van een Michelson interferometer kan als foutsignaal gebruikt worden om één der interferometerspiegels piezoelektrisch te positioneren op de gevoeligste plaats, voor kleine verplaatsingen.

VI. Het stabilisatiesysteem van een Michelson interferometer is met een kleine verandering ook bruikbaar in een capacitieve dilatometer.

1] hfdst. 2 van dit proefschrift.

2] K.Uchino, S.Nishida and S.Nomura,
A highly-sensitive AC interferometric
dilatometer, Jap.J. Appl.Phys. Vol. 21,
(1982), p.596-600.

3] K.Uchino and L.E.Cross, A very high sensitivity AC dilatometer for the direct measurement of piezoelectric and electrostrictive constants, Ferroelectrics, Vol. 27, (1980), p.35-39.

VII. Experimentatoren geven verschillende waarden van de gravitatieconstante, waarbij de foutengebieden om de opgegeven waarden, elkaar zelfs niet overlappen. Er moet hier sprake zijn van een onbekend effect.

G.T. Gillies, The Newtonian gravitational
constant: An index of measurements.

Rapport B.I.P.M.-82/9, uitgegeven door het

Bureau International des Poids et Measures,
Sèvres, France.

VIII. Bij het publiceren over nauwkeurige gravitatieconstante - experimenten is het noodzakelijk de tijdspanne te geven waarover de gemiddelde trillingstijd van de torsieslinger bepaald is. Op deze manier is het mogelijk de gemeten onzekerheid in de trillingstijd te vergelijken met de thermische ruis van deze slinger.

1] G.G. Luther and W.R. Towler, Redetermination of the Newtonian gravitational constant G , Phys.Rev. Lett., Vol. 48, (1982), p.121-123.

2] H.H.J.van Dijk, J.A.Poulis and F.N.Hooge, Noise in weighing, Appl. Sci. Res., Vol. 31, (1976), p. 445-453.

IX. De bewering dat Coulombkrachten de capaciteit van een geladen condensator doen toenemen is in zijn algemeenheid onjuist.

K.Küpfmüller, Einführung in die theoretische Elektrotechnik, 10^{de} druk, Berlijn: Springer Verlag, 1973.

X. "De Utrechtse opleiding richt zich meer op de relatie tussen de materialen en de fundamentele eigenschappen van de materie, terwijl de Technische Hogescholen meer gericht zijn op de technische aspecten van de productie".

Deze bewering, gedaan op blz. 129 van het ontwikkelingsplan 1983-1987 van de Rijks Universiteit Utrecht is niet geschikt als stelling, zelfs niet als laatste.

de T.H. gidsen.